Biological Journal of the Linnean Society, 2023, **138**, 249–273. With 9 figures.

Multilocus phylogeography, population genetics and niche evolution of Australian brown and black-tailed treecreepers (Aves: *Climacteris*)

SCOTT V. EDWARDS[1,2,*], JOÃO F. R. TONINI[1,2,3], NANCY MCINERNEY[4], COREY WELCH[5,7] and PETER BEERLI[6]

[1]*Museum of Comparative Zoology, Harvard University, Cambridge, MA 02138, USA*
[2]*Department of Organismic and Evolutionary Biology, Harvard University, Cambridge, MA 02138, USA*
[3]*Department of Biology, University of Richmond, Richmond, VA 23217, USA*
[4]*Smithsonian's National Zoo and Conservation Biology Institute, NW, Washington, DC 20008, USA*
[5]*Department of Biology and Burke Museum, University of Washington, Seattle, WA 98195, USA*
[6]*Department of Scientific Computing, Florida State University, Florida State University, Tallahassee, FL 32306, USA*
[7]*STEM Scholars Program, Student Innovation Center, Iowa State University, Ames, IA 50011, USA*

Received 18 July 2022; revised 24 October 2022; accepted for publication 28 October 2022

The Carpentarian barrier across north-eastern Australia is a major biogeographic barrier and a generator of biodiversity within the Australian Monsoonal Tropics. Here we present a continent-wide analysis of mitochondrial (control region) and autosomal (14 anonymous loci) sequence and indel variation and niche modelling of brown and black-tailed treecreepers (*Climacteris picumnus* and *Climacteris melanurus*), a clade with a classic distribution on either side of the Carpentarian barrier. mtDNA control region sequences exhibited reciprocal monophyly and strong differentiation (F_{st} = 0.91), and revealed a signature of a recent selective sweep in *C. picumnus*. A variety of tests support an isolation-with-migration model of divergence, albeit with low levels of gene flow across the Carpentarian barrier and a divergence time between species of ~1.7–2.8 Mya. Palaeoecological niche models show that both range size as measured by available habitat and estimated historical population sizes of both species declined in the past ~600 kyr and that the area of interspecific range overlap was never historically large, perhaps decreasing opportunities for extensive gene flow. The relatively long divergence time and low opportunity for gene flow may have facilitated speciation more so than in other co-distributed bird taxa across the Australian Monsoonal Tropics.

ADDITIONAL KEYWORDS: intron – neutrality – Pleistocene – stairway plot –selective sweep.

INTRODUCTION

Multilocus analyses of phylogeography and population history are now common for non-model species. Studies on non-model species have much to gain by learning from lessons, molecular markers, debates and conclusions advanced by studies in model species, such as humans. For example, soon after early studies of nuclear gene variation in human populations were completed, it became evident that some of the results from mitochondrial DNA might be idiosyncratic, and that a consideration of the differences in population history implied by the two types of markers could lead to novel insights (Fay *et al.*, 2001; Hey & Machado, 2003; Hey & Nielsen, 2004). Taking a different stance, many have suggested that the signals from mitochondrial DNA may be misleading for reconstructing population history, in so far as they exhibit signs of natural selection that could obscure the history that is the goal of inference (Hancock & Rienzo, 2008). The types and number of molecular markers employed in model species have been greatly expanded by the complete sequencing of genomes, and there has been increasing clarity as to the appropriate uses for different types of markers. As technology advances, genome-wide SNP analyses have come to dominate phylogeographic studies in both model and non-model

*Corresponding author. E-mail: sedwards@fas.harvard.edu

species, yet collections of unlinked SNPs provide only one lens through which to view population history. Alternative marker choices, such as resequencing of multiple sets of linked SNPs—so-called 'sequence-based markers', which include loci such as introns, exons and ultraconserved elements, offer additional windows into phylogeography and population history, particularly in their ability to estimate gene trees (Brito & Edwards, 2009; McCormack *et al.*, 2013, 2016). Gene trees can be challenging to estimate within species because of the paucity of sequence variation (Hare *et al.*, 1996; Hare & Avise, 1998), but have provided the foundation into a variety of recent analysis tools, allowing for a rich set of methods for hypothesis testing and parameter estimation and uncertainty at the species boundary (Beerli & Palczewski, 2010; Rannala & Yang, 2017; Flouri *et al.*, 2018, 2020; Beerli *et al.*, 2022). Such approaches are important in conservation planning (Unmack *et al.*, 2021) and have been employed extensively in phylogeography, including studies specifically on Australian birds and other biota (Jennings & Edwards, 2005; Lee *et al.*, 2012; Potter *et al.*, 2016, 2018; Oliver *et al.*, 2017; Edwards *et al.*, 2021).

The Carpentarian barrier (Fig. 1) is a major source generating biodiversity within the Australian Monsoonal Tropics (AMT: reviewed in Bowman *et al.*, 2010; Catullo *et al.*, 2014; Edwards *et al.*, 2016). The sources of vicariant splits across the AMT are still subject to speculation, but include a variety of Pleistocene environmental changes; intrusions of the sea, desertification and vegetation turnover have likely

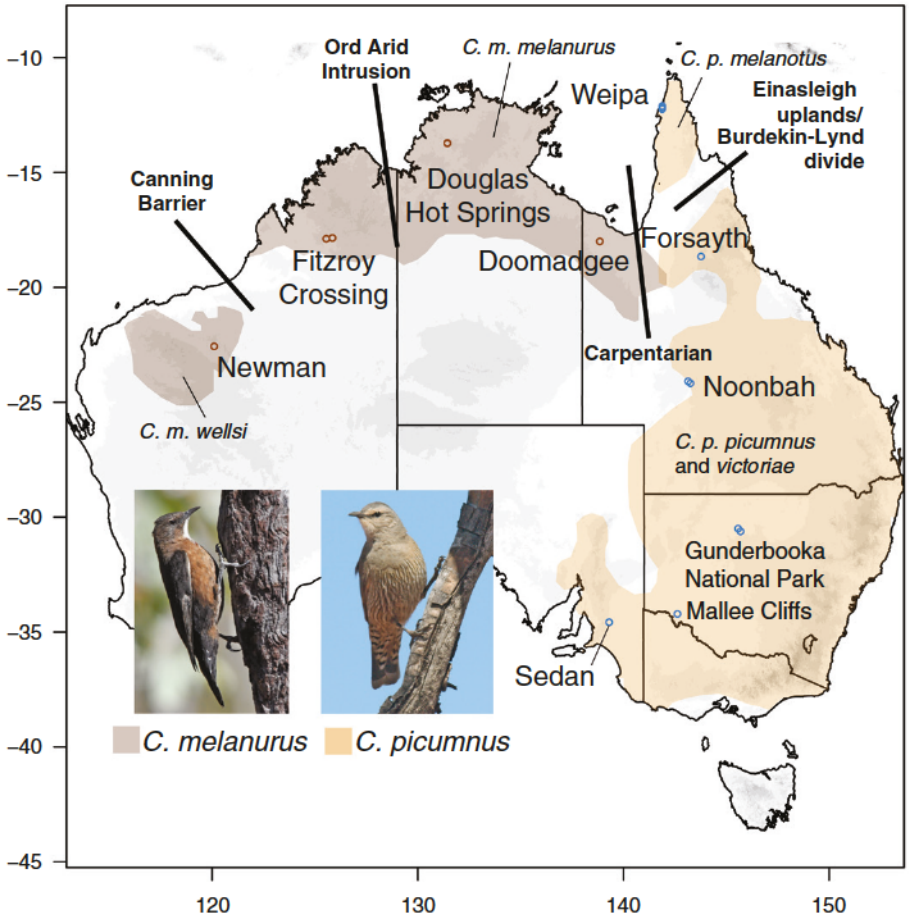

Figure 1. Location of treecreeper specimens and geographic range of *C. picumnus* and *C. melanurus*. Point samples of treecreepers were taken at each locality and deposited in the University of Washington Burke Museum, except for the samples from Sedan, South Australia, which came from the South Australian Museum. Samples from Mallee Cliffs were used only for the mitochondrial control region sequences. Multiple micro-localities within major localities were lumped for purposes of reporting results. Latitude and longitude of each sample can be found in the Supporting Information (Table S1) and at the University of Washington Burke Museum Ornithology database. Photos courtesy of and copyright of Graeme Chapman. *Climacteris melanurus* taken ~244 km south of Doomadgee, Queensland (-20.31 °N, 139.14 °W); *C. picumnus* taken ~195 km south of Forsayth, Queensland (-20.41 °N, 143.55 °W).

all contributed to its status as a biological barrier (Reeves *et al.*, 2013; Ewart *et al.*, 2020). Ecological niche modelling has shown that, for many AMT bird species surveyed thus far, the expected niche as estimated from biodiversity records or specimens extends fully across the Carpentarian barrier, with sometimes extensive fluctuations on the southern extent of the estimated range (Dorrington *et al.*, 2020). This pattern is consistent with many of those species being relatively undifferentiated, or showing differentiation to the level of subspecies, such as the blue-winged kookaburra (*Dacelo leachii*) or the grey shrike-thrush (*Colluricincla harmonica*), respectively (Lamb *et al.*, 2019; Dorrington *et al.*, 2020). Additional examples of phylogeographic surveys of low-differentiated AMT species, or more widespread species with a strong AMT component, include the red-backed fairy wren (*Malurus melanocephalus*: Lee & Edwards, 2008), grey-crowned babblers (*Pomatostomus temporalis*: Edwards, 1993), butcherbirds (*Cracticus*: Kearns *et al.*, 2014), and several species of honeyeater (Meliphagidae: Peñalba *et al.*, 2019; reviewed in Dorrington *et al.*, 2020; Burley *et al.*, 2022). As in many vicariant patterns across the globe, patterns of divergence across the Carpentarian barrier are variable: some species exhibit deeper divergences and rates of reciprocal monophyly of gene trees than others (Edwards *et al.*, 2016; Peñalba *et al.*, 2019). This variation in divergence time could be caused by variable histories of range overlap, current connectivity and geographic distance, all contributing the speciation process.

Here we combine inference from mtDNA with a multilocus coalescent approach to analysing variation at anonymous nuclear noncoding loci on a continent-wide scale across populations of treecreepers in the genus *Climacteris*. The genus *Climacteris* is phylogenetically distinctive, comprising one of the deepest branching lineages in the Corvida, a large radiation of passerine birds with roots deep in Australia and New Guinea, and ultimately Gondwana (Oliveros *et al.*, 2019). We chose the brown (*Climacteris picumnus*) and black-tailed (*Climacteris melanurus*) treecreepers to study because, together with the rufous treecreeper (*Climacteris rufus*) of southern Australia, they provide a classic case of speciation in Australia: their range spans all the major areas of endemism identified in previous works (Keast, 1957; Cracraft, 1986), a pattern that provides the foundation for many scenarios of community divergence and speciation in Australia (reviewed in Edwards *et al.*, 2016). *Climacteris* treecreepers therefore provide an important test case of biogeographic scenarios of other Australian birds for which mitochondrial and nuclear DNA analyses have been conducted (Lee & Edwards, 2008; Kearns *et al.*, 2014; Peñalba *et al.*, 2017, 2019; Dorrington *et al.*, 2020). The two species inhabiting the AMT are entirely allopatric today, yet their ranges approach each other in the region of the Carpentarian barrier just inland from the Gulf of Carpentaria in northern Queensland (Fig. 1). Both their geographic range and preliminary phylogenetic studies suggest that they are sister taxa (Cracraft, 1986), allowing us to study both population differentiation, species divergence and gene flow comprehensively in this system. Moreover, treecreepers span at least two additional major biogeographic breaks that have been highlighted in biogeographic and phylogeographic studies of Australian birds and other taxa (Fig. 1: Doughty *et al.*, 2011; Eldridge *et al.*, 2012; Lamb *et al.*, 2019): the Canning barrier in *C. melanurus*, separating populations in the Pilbara region and those in the Kimberley in north-west Australia, and the Black Mountain Corridor and other breaks in *C. picumnus* in the eastern forests (Cracraft, 1986; Lee & Edwards, 2008; Bryant & Krosch, 2016). The Cape York Peninsula population of *C. picumnus* has been recognized as a subspecies (*Climacteris picumnus melanotus*) by several authorities and is darker and smaller than more southerly populations (Keast, 1957). The phenotypically distinctive Pilbara population of *C. melanurus* has also been recognized as subspecifically as *Climacteris melanurus wellsi* (Keast, 1957; Ford, 1987), forming with *C. picumnus* a distinct pattern of allopatrically replacing populations around the periphery of north-western, northern and eastern Australia. Indeed, speaking from a perspective dominated by Pleistocene speciation time frames, Keast (1961: 375) stated that '*Climacteris* provides one of the best demonstrations of differentiation and speciation in refugial areas'.

Climacteris treecreepers inhabit a range of environmental regimes known to influence patterns of differentiation in other taxa and span multiple biogeographic barriers seen in other taxa, thereby allowing for tests of phylogeographic congruence in a predictive framework. Multiple phylogeographic systems have been studied in the Kimberley, a region of increasing microendemism discovery, particularly among lizards and skinks (Oliver *et al.*, 2017; Silva *et al.*, 2017; Doughty *et al.*, 2018; Potter *et al.*, 2018; Rosauer *et al.*, 2018). By contrast, the Pilbara, although known as a region of 'exceptionally high biotic diversity and endemism' (Pepper *et al.*, 2013b), driven by ancient and unusual soils, varied topography and long-term geological stability, is less well studied phylogeographically, especially for birds (Edwards, 1993; Doughty *et al.*, 2011; Pepper *et al.*, 2011, 2013a; Eldridge *et al.*, 2012). In addition to expecting strong differentiation between the two species across the Carpentarian barrier, we might also predict the strongest genetic differentiation within species between Pilbara populations and those from the Top End and Kimberley, produced by the Canning barrier,

with less differentiation across other intraspecific barriers, such as the Black Mountain Corridor and adjacent barriers in the east and the Ord River region barriers between Kimberley and Top End (Ford, 1978; Bryant & Krosch, 2016; Edwards *et al.*, 2017; Peñalba *et al.*, 2017; Flores-Rentería *et al.*, 2021).

As is typical of Australian passerines, *Climacteris* treecreepers are long-lived for their body size; the maximum longevity of *C. picumnus* is recorded at 13 years, 11 months (Bird *et al.*, 2020). Whereas female brown treecreepers mostly breed in their first year, average age at first breeding for males is nearly 3 years (Doerr & Doerr, 2006); a statistical analysis yields a surprisingly long generation time of 5 years for this species (Bird *et al.*, 2020). These life history details and generation time have important consequences for the estimation of species divergence times (Bakker *et al.*, 2022; Jonasson *et al.*, 2022). Both *C. picumnus* and *C. melanurus* are cooperatively breeding species: individuals typically occur in family groups consisting of three to five individuals including presumed parents and young aiding the recruitment of the next generation (Doerr & Doerr, 2006, 2007; Bennett *et al.*, 2012b). Cooperatively breeding species are often thought to have low dispersal rates (Rusk *et al.*, 2013), and estimation of gene flow with genetic markers in such species can yield insight into the long-term consequences of dispersal between populations as estimated from field-based studies (Edwards, 1993; Painter *et al.*, 2000; Bertrand *et al.*, 2014), as well as aid in conservation measures, which are particularly acute for treecreepers in north-east New South Wales and in the Cape York Peninsula (Ford *et al.*, 2009; Bennett *et al.*, 2012a).

Climacteris treecreepers have also figured prominently in areas of population genetic and mitochondrial adaptation. In a survey of 17 species of Australian songbirds (oscines), Lamb *et al.* (2018) found that the brown treecreeper, *C. picumnus*, displayed high differentiation between the Cape York Peninsula and more southerly populations in the *ND2* gene, and that *C. picumnus* was among the few ($N = 6$) species where climate explained significant *ND2* variation after geography was factored out. Although they also employed codon models to understand natural selection on mitogenomes at the macroevolutionary level among Australian songbirds, no microevolutionary tests of mtDNA variation or analyses of nuclear DNA were performed. Our continent-wide multilocus survey of nuclear and mitochondrial diversity in treecreepers therefore can further address the extent of natural selection in *C. picumnus* and potentially *C. melanurus*. The data set presented here has been analysed briefly in other contexts (Balakrishnan *et al.*, 2010; Edwards *et al.*, 2016), but has otherwise not been presented in full detail. Additionally, we combine estimates of population size changes over time with niche models (Knowles *et al.*, 2007; Stiels & Schidelko, 2018) to understand what if any connection there was between available palaeoclimates, available land area and genetic diversity in the past (Joseph *et al.*, 2019; Peñalba *et al.*, 2019; Burley *et al.*, 2022). These studies will add to the database of divergence across the periphery of Australia and the genetic diversity of Australian vertebrates in general (Edwards *et al.*, 2016).

MATERIAL AND METHODS

FIELDWORK, SAMPLING AND TAXA STUDIED

Specimens for this study were collected and prepared as voucher museum specimens over several field trips conducted from 1996–2002 under the appropriate permits. Tissue samples were borrowed from existing collections to supplement fieldwork (Fig. 1; Supporting Information, Table S1). Tissues were sampled from individuals and stored in liquid nitrogen in the field, and stored long term at -80 °C at the Burke Museum, University of Washington. Additional details and justification of our sampling scheme are provided in the Supporting Information, Text S1).

DNA ISOLATION, PRIMER DEVELOPMENT AND RESEQUENCING

Total genomic DNA was extracted from heart, liver or muscle tissue using phenol chloroform methods. Details of PCR conditions for mtDNA amplification can be found in Supporting Information, Text S1. To generate nuclear loci, we constructed a plasmid library from total genomic DNA from a single female *C. picumnus*, shearing, repairing and size-selecting the DNA into 2–3 kb fragments using methods outlined in Jennings & Edwards (2005). The sized fragments were cloned into a puc18 vector, transformed into competent *E. coli* DH10B cells (Invitrogen), and plated on agarose. Additional details on cloning protocol, PCR conditions and characterization of anonymous loci using the Aliview (Larsson, 2014), Polyphred (Nickerson *et al.*, 1997), Coding Potential Calculator2 and MISA microsatellite finder (Beier *et al.*, 2017) web servers can be found in Supporting Information, Text S1.

HAPLOTYPE RESOLUTION, GENETIC DIVERSITY AND POPULATION STRUCTURE

Unphased diploid DNA sequences for each locus were phased using Phase 2.0 (Stephens *et al.*, 2001). We accepted as valid the haplotype set with the highest likelihood, with the two haplotypes for each

locus labelled as 'a' and 'b'. Phased haplotypes were converted into Nexus (Maddison *et al.*, 1997) and Phylip (Felsenstein, 1994) formats for subsequent analyses, and Paup* (Swofford, 2002) and PGDSpider (Lischer & Excoffier, 2011) were used for routine file format conversions. Standard population genetic statistics, such as genetic diversity within and between populations and species (π, Nei & Li, 1979), Tajima's D (Tajima, 1989) and F_{st} among populations based on pairwise differences of haplotypes (Hudson *et al.*, 1992), were calculated using the R package PopGenome v.2.7.5 (Pfeifer *et al.*, 2014). Gene trees were constructed using the maximum likelihood algorithm in IQ-TREE v.1.6.12 (Nguyen *et al.*, 2015), using best substitution models for each locus as estimated in ModelFinder (Kalyaanamoorthy *et al.*, 2017) and the Bayesian Information Criterion. Net nucleotide diversity between populations and species [$D = d_{xy} - 0.5(d_x + d_y)$, Nei & Li, 1979], was calculated using PopGenome (Pfeifer *et al.*, 2014). Indels were scored as biallelic or multiallelic and the F_{st} for each indel was calculated using the hierarchical method of Yang (1998) as implemented in hier*F*stat (Goudet, 2005). We analysed the data via principal components analysis (PCA) in smartpca v.8000 (Patterson *et al.*, 2006), in part to detect potential outliers and sequencing errors but, more importantly, to determine if the PCA plot could reveal details of population structure (Novembre *et al.*, 2008). We used STRUCTURE v.2.3.2.1 (Pritchard *et al.*, 2000) to understand the basic population units within and between species. Details of STRUCTURE runs and analysis (Evanno *et al.*, 2005; Earl & vonHoldt, 2012), as well as additional simulations using ms (Hudson, 2002) and the number of interspecific coalescent events (Fitch, 1971; Slatkin & Maddison, 1989; Takahata, 1989; Maddison & Maddison, 2019) can be found in the Supporting Information (Text S1).

Hypothesis testing with gene tree variation

Gene trees were tested against a priori hypotheses of species and population monophyly using the approximately unbiased (AU) and Kishino–Hasegawa tests (Shimodaira, 2002) with 1000 bootstraps as implemented in IQ-TREE. Specifically, to explore the extent of significant variation among gene trees, we asked whether the data from the alignment of each locus could reject the trees from the other 14 alignments. We used Phrapl (Carstens *et al.*, 2017; Jackson *et al.*, 2017) to test hypotheses of major classes of phylogeographic models in treecreepers. Phrapl takes a set of rooted gene trees and, using AIC, tests them against the coalescent expectations of a suite of models built from different combinations of population parameters, including directional gene flow, changes in population size, and divergence of populations. Although the sequence data is not interrogated in such tests, the results can help narrow down the number of models. Additional details on our use of Phrapl can be found in the Supporting Information, Text S1.

Divergence models with and without gene flow

We used bpp v.4.3 (Yang & Rannala, 2010; Flouri *et al.*, 2018, 2020) to estimate the population phylogeny and divergence times among *Climacteris* populations. We pruned the data to include only 54 individuals with high representation of unambiguous sites within loci. Informed by the population genetic analyses, we used the parameter estimation mode A00 to estimate population divergence times and effective population sizes given an assumed phylogeny with four tips: the Newman/Pilbara population of *C. melanurus* (subspecies *wellsi*), the remaining Top End populations of *C. melanurus*, the Weipa population of *C. picumnus* (subspecies *melanotus*) as well as the remaining *C. picumnus* populations. We ran bpp with both a single rate and multiple rates across loci, implementing the best substitution models for each locus using the output from IQ-TREE. We also tested models of divergence with gene flow, assuming gene flow occurred only between the easternmost clade of *C. melanurus* (all but Newman) and the non-Weipa *C. picumnus* populations. These analyses permitted estimation of the time of the single pulse of gene flow and the probability of gene flow during that pulse (Flouri *et al.*, 2020). We ran 800 000 cycles, sampling every second cycle. Additional details of bpp runs can be found in the Supporting Information, Text S1. We summarized the mcmc output in Tracer (Rambaut *et al.*, 2018) and the coda R package (Plummer *et al.*, 2006).

We used migrate-n (v.5.0, Beerli & Felsenstein, 1999; Beerli, 2006) to conduct additional phylogeographic model selection (divergence with gene flow) using the full data set as well as equilibrium models of gene flow within *C. picumnus* and *C. melanurus* separately. All analyses were run in Bayesian mode and in parallel across 30–480 cores with a static heating scheme across four chains (1M, 3, 1.5 and 1) that allowed for thermodynamic integration with Bezier smoothing during Bayes factor analysis (Beerli & Palczewski, 2010). We used flat priors for each parameter, except for two additional runs of the isolation-migration model, where we used an exponential prior on divergence time, with means of 0.001 and 0.01. Each analysis was run in replicate between 10 and 32 times to check average results from across the runs. We evaluated six equilibrium migration models per species using the Bayesian framework in migrate-n. We first analysed a series of models within each species, starting with

a single panmictic population, then several models with two major populations and differing by the pattern of symmetrical or asymmetrical gene flow, and finally, maximally complex models with four and five populations for *melanurus* and *picumnus*, respectively (Supporting Information, Fig. S11). mtDNA data was not included in these analyses. Model selection was conducted using Bayes factors as described in Beerli & Palczewski (2010).

The between-species analyses utilized the full sequence data from *C. picumnus* and *C. melanurus*, treating each species as a panmictic population. The population structure within each species should not have any obvious effects on divergence times between species—our main parameter of interest here. The violation of the panmixis assumption will likely cause the value of θ for each species to be higher than if each species were modelled as a subpopulation, but it does not misrepresent the biology, since the effective population size of a structured species has a known and predictable relationship to that of a panmictic species with the same total number of breeding individuals (Nei & Takahata, 1993). Using a novel framework incorporating population divergence (Beerli *et al.*, 2022), we developed eight two-species models involving population divergence and gene flow, with and without a putative ancestral population from which extant sampled populations emerged, as well as a pure equilibrium migration model (Supporting Information, Fig. S12). Incorporation of an unsampled ancestral population allows one to test models in which both extant populations diverged from each other at the same time, as opposed to one population being derived from another (Beerli *et al.*, 2022). Without a putative ancestral population, population divergence is assumed to follow a pattern in which one extant species served as an ancestral population from which the other sampled species diverged (so-called 'budding speciation': Caetano & Quental, 2022). Whereas bpp assumes a single pulse with a particular probability of gene flow between designated populations, migrate-n assumes continuous gene flow initiating immediately after population divergence.

For all demographic analyses, we converted species and population divergence times to years and genetic diversity (θ) to effective population sizes by assuming a mutation rate ± 1 SD of $2.2 \times 10^{-9} \pm 0.2 \times 10^{-9}$ and a generation time of 2 ± 0.2 years. The mutation rate we used, appropriate for noncoding DNA and used in other bird studies (Termignoni-García *et al.*, 2022), came from an estimate based on calibrations of four-fold degenerate sites in proteins between zebra finch, chicken and other amniotes with known divergence time (Nam *et al.*, 2010). Two years is a reasonable estimate of the average age at first breeding in *C. picumnus* (Doerr & Doerr, 2006) and likely *C. melanurus*, but we also used 5 years as an estimate of generation time for these species based on demography (Bird *et al.*, 2020). For the bpp analyses, the uncertainty of the mutation rate and generation time were modelled as a gamma distribution and contribute to the 95% confidence intervals (CI) of the Bayesian output using the bbpr R script (Angelis & dos Reis, 2015).

Species distribution models and changes in population size through time

We generated species distribution models for all species in the data set to understand the potential for gene flow between species via range overlaps over time, and also to understand how closely effective population sizes over time were correlated with estimates of ancestral niche areas. We supplemented the localities used for the genetic data (Supporting Information, Table S1) by downloading locality information from the Global Biodiversity Information Facility (GBIF; https://www.gbif.org/) on 31 March 2020 using the package *rgbif* (Chamberlain *et al.*, 2021) in R (R Core Team, 2019).

For each species, we used ENMeval (Muscarella *et al.*, 2014) to test the best model parameters for downstream analysis with Maxent v.3.4.1. Ecological niche models are subject to a number of biases, including those related to the different models, tuning parameters and data set sizes (Warren *et al.*, 2021). ENMeval, which we use here to estimate species distribution models (SDMs), incorporates model tuning for Maxent into the analysis, a facility not found in all packages. The ENMevaluate function was set up to use Maxent 3.4.1 (Phillips *et al.*, 2017) in the package dismo (Hijmans *et al.*, 2011) and the climatic data used is from the PaleoClim database (Brown *et al.*, 2018). Additional details of filtering of GBIF data using *CoordinateCleaner* (Zizka *et al.*, 2019) and use of feature classes and training of the model can be found in Supporting Information, Text S1.

We used Stairway plots (Liu & Fu, 2015, 2020) to estimate variation in effective population size through time for *C. picumnus* and *C. melanurus* and to test the hypothesis that effective population size through time was correlated with available habitat through time as estimated with ENMeval. The Stairway plot is a composite likelihood method that uses the folded or unfolded site frequency spectrum (SFS) to estimate changes in the mutation-scaled population size θ for a variable number of 'epochs' in coalescent trees. Stairway assumes a random-mating population; we tested Stairway plots with and without the main outlier populations within *C. picumnus* (Weipa) and *C. melanurus* (Newman) and found little difference, and so we used the entire data sets for each species to generate SFSs. We estimated the unfolded site frequency spectrum from all autosomal loci, using a

single allele from *C. rufus* as an outgroup. We also examined results using the folded SFS, to see if the results were robust to the data type and also because our unfolded SFS could be biased by the specific outgroup that we chose. Stairway plots were run using default search parameters, including four random break start points at 7, 15, 22 and 28, and allotting 67% of the sites for training (additional details in Supporting Information, Text S1).

RESULTS

Locus diversity, population structure and summary statistics

We sequenced 367 bp of mitochondrial control region (CR) 1 for 48 *C. picumnus*, 46 *C. melanurus* and 14 outgroup individuals, totalling 108. There was a total of 80 variable sites among all taxa, and 28 variable sites among *C. picumnus* and *C. melanurus*. A maximum likelihood gene tree showed reciprocal monophyly of *C. picumnus* and *C. melanurus*, with four sequences from the Weipa population of *C. picumnus* clustering separately from the remaining *picumnus* (Supporting Information, Figs S1–S2). In the consensus bootstrap tree, these same four sequences cluster weakly (50%) as sister to the *melanurus* sequences (Supporting Information, Figs S1–S2). Tree-topology tests in IQ-TREE (Supporting Information, Table S3) indicated that reciprocal monophyly of *C. picumnus* and *C. melanurus* sequences could not be rejected ($P = 0.91$), although the topology was ultimately sensitive to the alignment of the 3' end of the sequence and there was relatively little information in these short CR sequences.

We successfully cloned 14 anonymous nuclear loci (AL) as templates for PCR amplification. We originally conducted a BLAST analysis of all 14 candidate loci immediately after cloning (in 2004) to determine functions of our putatively anonymous loci or to help inform modelling of substitutions. We found that none of them matched sequences in the database. Upon repeating the BLAST analysis during the final data analysis on 24 March 2020, four of the 14 loci elicited a significant hit to various sequences in the database (Supporting Information, Table S2). These sequences all had matches to avian genomes [often to sequences in kiwis (*Apteryx*) or eagles (*Aquila*)] and included a number of repetitive sequences, including WD repeats (AL21), HEAT5A repeats (AL16, AL32) or to anonymous, unannotated regions (AL18, AL20) of various genome assemblies. The coding potential of each locus, as assessed by CPC2 (Kang *et al.*, 2017), was uniformly low, with all loci being designated as 'non-coding' with open reading frame integrity scores of less than 0.15. Each locus cleanly amplified a single PCR product and upon sequencing yielded clear sequences with readily identifiable heterozygous sites. We therefore proceeded with sequencing these loci across the collected individuals. Alignment lengths of each locus varied from 288 to 418 base pairs (bp, mean = 356.93, ± 1 SD = 33.73 bp) and the GC-content of each locus averaged across individuals varied from 0.350 to 0.608 among loci (mean across all individuals 0.469 ± 0.077; Supporting Information, Table S3). These GC values are typical for bird genomes. Within species, the number of biallelic SNPs per locus varied from 1 to 20, whereas both species had a low incidence of polyallelic sites (three nucleotides; maximum two per locus, average 0.167 per locus; Supporting Information, Table S3). Within individual populations, the number of SNPs per locus varied from 0 to 15, with no polyallelic SNPs within any one population.

Gene tree heterogeneity and lineage sorting

Maximum likelihood gene trees varied in their implications for treecreeper phylogeography (Supporting Information, Fig. S3). None of the gene trees implied monophyly of either *C. picumnus* or *C. melanurus* alleles (Supporting Information, Fig. S3). The outgroup sequences from *C. affinis* and *C. rufa* were monophyletic in only five of the 15 gene trees (Supporting Information, Table S3). Several cases of identical sequences occurred among *C. picumnus*, *C. melanurus* and the outgroup sequences. Considering alleles only from *C. picumnus* and *C. melanurus*, the number of interpopulation coalescent events varied from 2 to 21, with a mean of 6.93 (Supporting Information, Table S3). Using approximately unbiased (AU) tests, we found that in most cases, there was significant conflict between loci, both with the topologies of other loci and with a gene tree exhibiting reciprocal monophyly within each species (Supporting Information, Fig. S4). The sequence data for the loci AL7, AL14, AL22 and AL32 in particular were in strong conflict with topologies from other loci. Simulations using ms (Supporting Information, Fig. S5; Text S1), as well as the results of the Phrapl analysis (Supporting Information, Table S4) suggested that interspecific gene flow likely shaped these genes trees in addition to incomplete lineage sorting, a conclusion that informed our downstream analyses.

Population structure, divergence and neutrality

The extent of nucleotide diversity (π) varied substantially and significantly among populations ($P < 0.05$) and loci ($P < 0.05$), and between nuclear DNA and mtDNA (Fig. 2A, B). Whereas one population (Newman) had no variation at mtDNA, all populations

exhibited some variation at anonymous loci. In general, nucleotide diversity for anonymous loci exceeded that for mtDNA in all populations except Weipa (Fig. 2A, B). Anonymous locus AL22 exhibited over eight times greater diversity than AL5 [Fig. 2; $F_{(13,\ 112)} = 11.34$, $P = 3.55\text{e-}15$, $\eta^2_p = 0.57$, 90% CI (0.47, 1.00)]. The diversity at each nuclear locus and at mtDNA was highly correlated between the two species [$t = 3.9552$, d.f. = 13, $P = 0.0016$, Pearson's rho = 0.739, 90% CI (0.441, 0.890), Fig. 2D].

The level of differentiation among populations, as measured by F_{st} and d_{xy}, indicated that, within *C. melanurus* and overall, the Newman population in the Pilbara was the most differentiated, with an average nuclear and mitochondrial F_{st} with other *C. melanurus* populations of 0.289 and 0.90, respectively (Fig. 3; Supporting Information, Figs S6–S7). Within *C. picumnus*, the Weipa population was the most differentiated, with an average nuclear and mitochondrial F_{st} with other *C. picumnus* populations of 0.105 and 0.217, respectively, slightly higher than differentiation exhibited by the Mallee Cliffs population. D_{xy} showed similar patterns of differentiation, although was more uniform than F_{st} for nuclear DNA within both

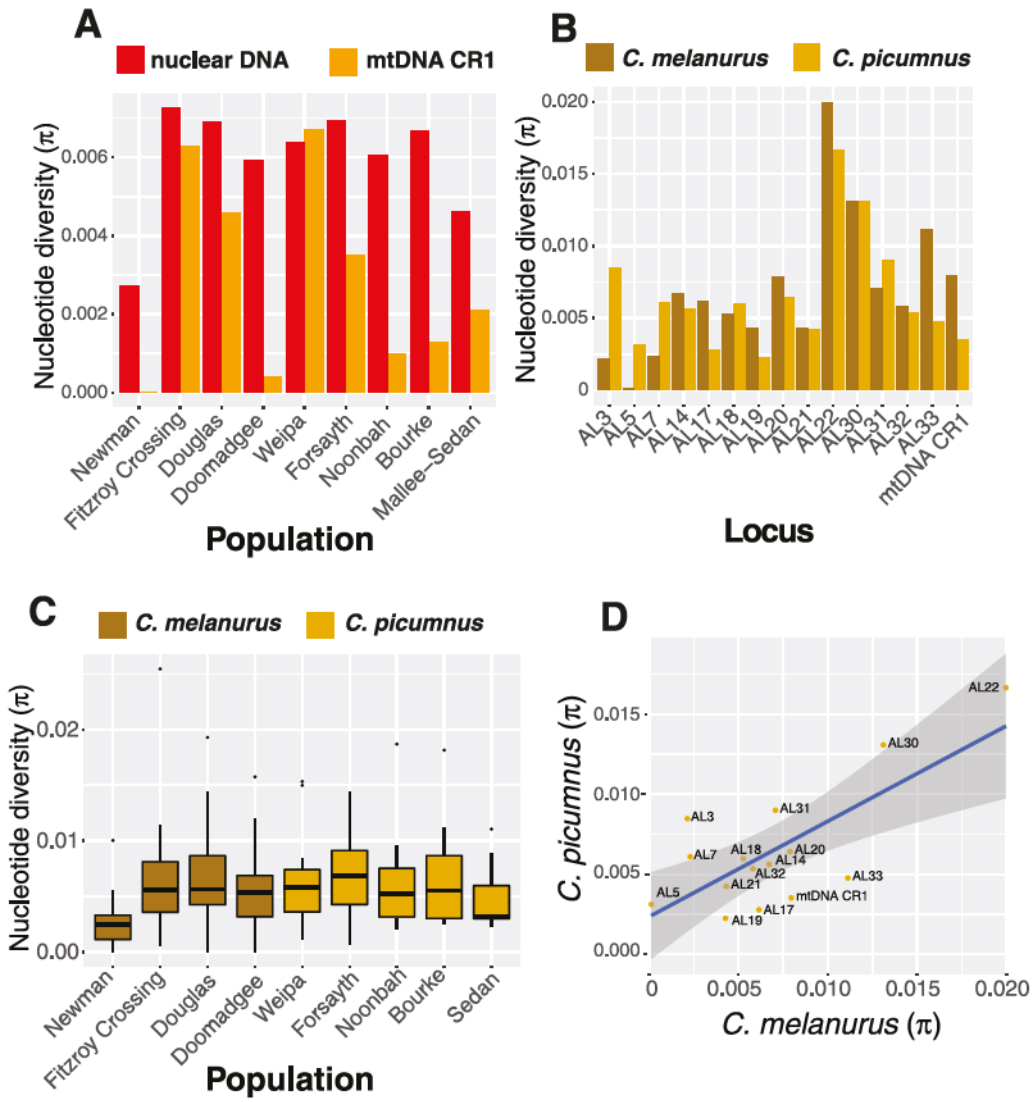

Figure 2. Patterns of nuclear and mitochondrial genetic diversity in *C. picumnus* and *C. melanurus*. A, mtDNA CR1 nucleotide diversity and average nucleotide diversity for the 14 anonymous (AL) loci of each population of *C. picumnus* and *C. melanurus*. Populations are arranged west on the left to east/south on the right of the *x*-axis. B, nucleotide diversity by locus averaged across all populations of *C. picumnus* and *C. melanurus*. C, average nucleotide diversity presented as box plots for each population of *C. picumnus* and *C. melanurus*. D, correlation of nucleotide diversity for each locus between *C. picumnus* and *C. melanurus*.

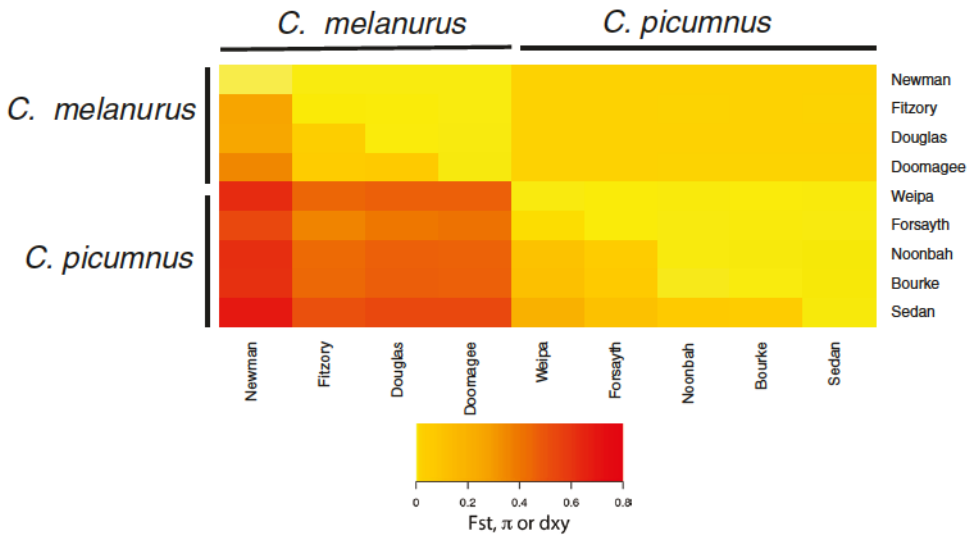

Figure 3. Heatmap of F_{st} (below diagonal) and d_{xy} (above diagonal) for populations of *C. picumnus* and *C. melanurus* for 14 anonymous loci. Nucleotide diversity for each population is presented along the diagonal. Populations are ordered from west to east going left to right or top to bottom for *C. melanurus* and *C. picumnus*. For precise values of each statistic see Supporting Information, Fig. S7.

picumnus and *C. melanurus*, and for mtDNA within *C. picumnus* (Supporting Information, Figs S6–S7).

Principal components analysis (PCA) using smartpca and STRUCTURE both reinforced the conclusions from F_{st} (Fig. 4). PCA revealed a striking pattern in which the individuals and populations were arrayed across the plot in a way that mirrored their relative geographic locations across Australia, with a clear 'east-west' separation between *C. melanurus* and *picumnus* along PC1, which explained 24.89% of the genetic variation, and a 'north-south' variation within each species along PC2, which explained 5.94% (Fig. 4A). Newman was again the most differentiated, with no overlap with other populations. Slight clinal variation along PC2 is evident within *C. picumnus*. Tracy–Widom statistics indicated that the first five PCs were significant ($P < 0.05$). STRUCTURE analysis showed a clear separation of *C. melanurus* and *picumnus*, with little evidence for individuals belonging to multiple genetic groups (Fig. 4B). When each species was analysed alone, additional substructuring was evident, with Newman again appearing differentiated relative to other *melanurus* and Weipa showing the most differentiation within *picumnus*. K = 2 was the optimal number of genetic groups for all three analyses (Fig. 4B).

We used Tajima's *D* to test for neutrality of mtDNA CR1 sequences and anonymous loci (Fig. 5). CR1 yielded a significantly negative Tajima's *D*, as did one locus (AL32) in *C. picumnus* and two loci (AL3, AL19) in *C. melanurus*. The average Tajima's *D* across nuclear loci for both species was slightly negative (-0.426, *C. picumnus*; -0.328, *C. melanurus*).

INDEL AND MICROSATELLITE LENGTH VARIATION CORROBORATE GEOGRAPHIC PATTERNS OF DIFFERENTIATION

We found 21 examples of indels among the anonymous loci, varying in length from 1 to 25 bp (Fig. 6; Supporting Information, Table S5). Six of these indels were invariant within *C. picumnus* and *C. melanurus*, and varied only in comparison to outgroups. The 15 indels polymorphic within *C. picumnus* and *C. melanurus* displayed a wide diversity of geographic patterns, and generally corroborated patterns of diversity suggested by the sequence-based gene trees. Some indels showed strong, near complete differentiation between *C. picumnus* and *C. melanurus*, or were restricted to specific areas of endemism around the continent, such as indels 15 and 6, respectively (Fig. 6A, C). Others showed less population structure, or possibly microevolutionary convergence. For example, indel 9 in AL20 is a 4-bp microsatellite repeat where the derived condition, based on comparisons with outgroups, is likely deletion of a repeat unit (Fig. 6B). This condition is found in five of the eight populations and in both species, yet the Newman, Cape York Peninsula and Sedan populations all retain the ancestral state (insertion). All but one indel polymorphisms were biallelic, with indel 20, a mononucleotide repeat varying from 5 to 10 bp, displaying six alleles (Fig. 6D). Overall, the level of among-population differentiation of indels was slightly higher than that for SNPs (Supporting Information, Fig. S8).

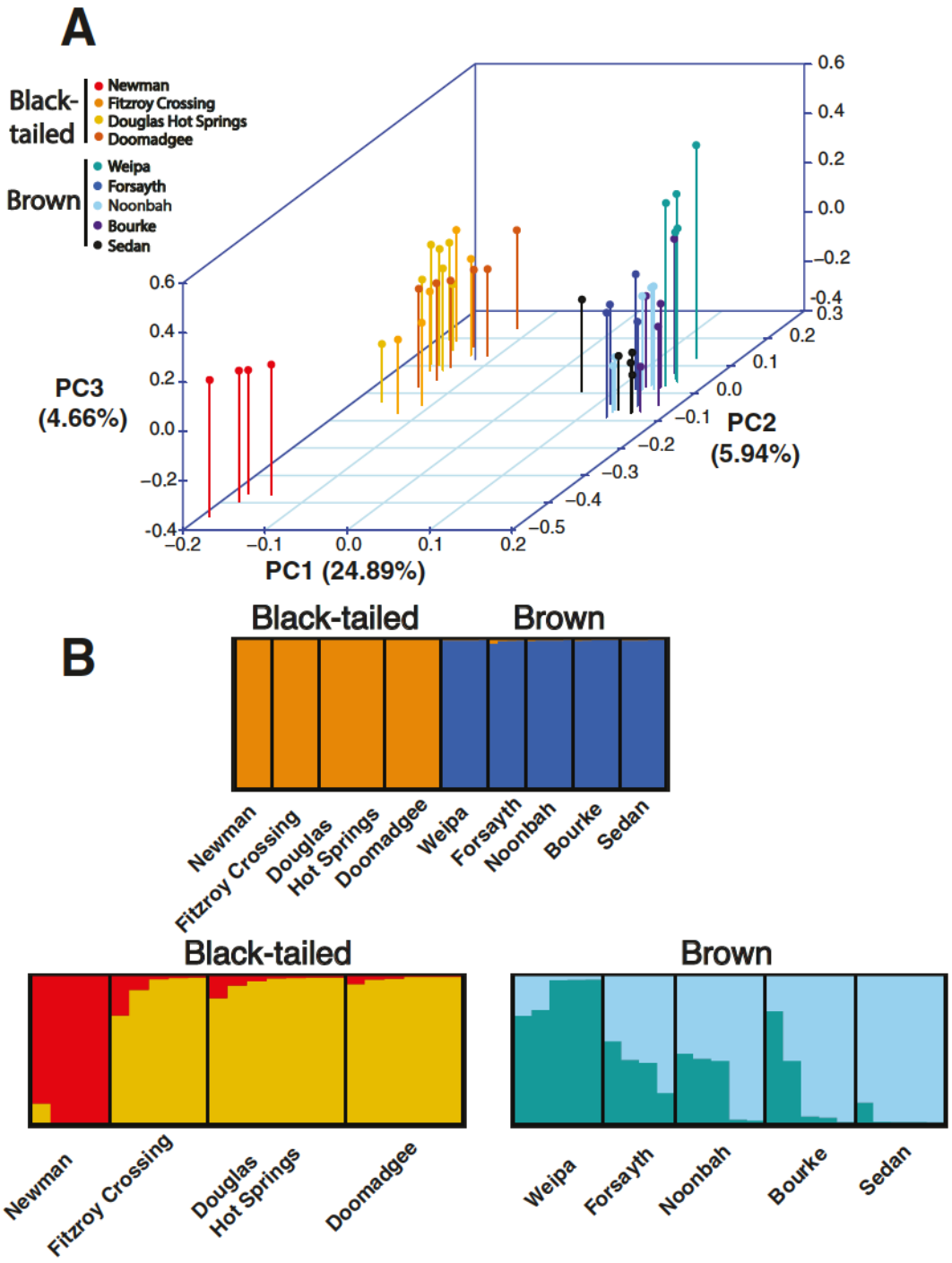

Figure 4. Population structure within *C. melanurus* and *C. picumnus* revealed by PCA and Structure. A, PCA plot of all individuals within *C. melanurus* and *C. picumnus* for the first three principal components. Populations are colour-coded by key at upper left. B, above, Structure plot (k = 2) for combined analysis of *C. melanurus* (black-tailed) and *C. picumnus* (brown); below, Structure plot, k = 2, for each of *C. melanurus* and *C. picumnus* separately.

POPULATION DIVERGENCE TIMES AND LOCUS RATE HETEROGENEITY USING BPP

We assessed phylogenetic relationships among *Climacteris* populations using bpp applied to nuclear loci only. To focus on divergence among major lineages, we assumed a tree with only two sister lineages within each species: Newman within *C. melanurus* and Weipa within *C. picumnus* (Supporting Information, Fig. S9).

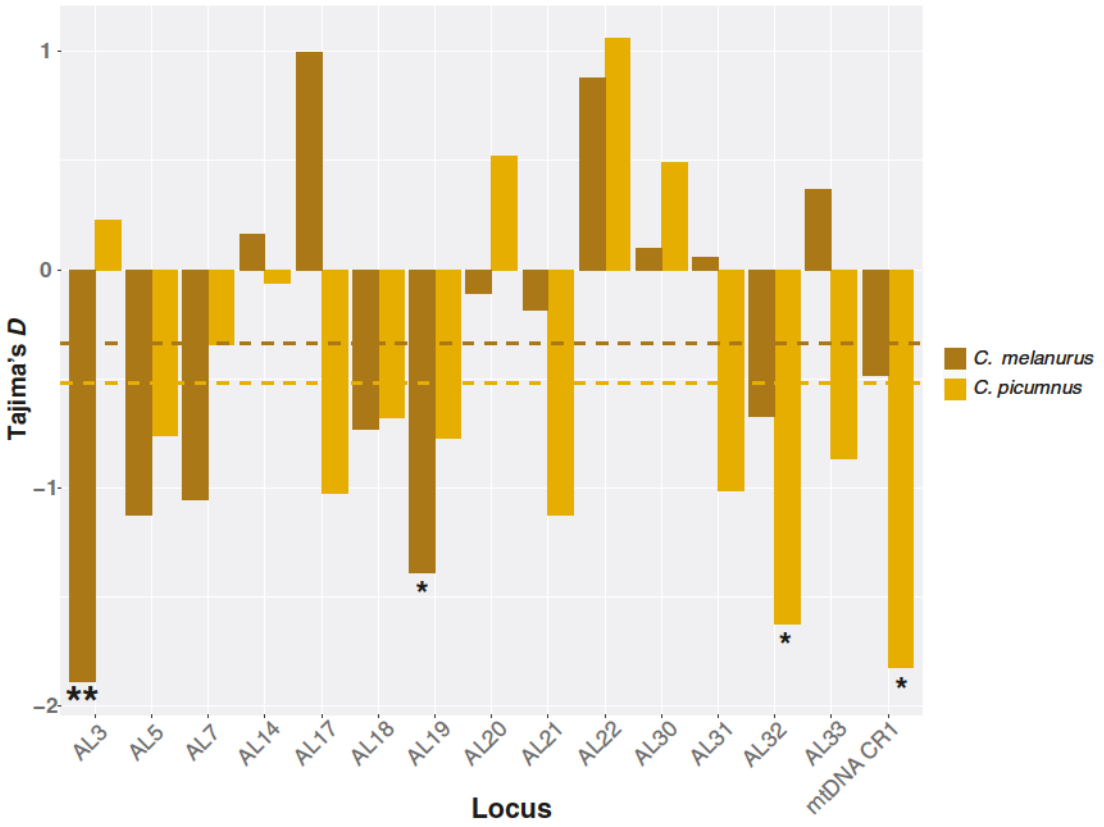

Figure 5. Estimates of Tajima's *D* for 14 anonymous loci and mtDNA CR1 within *C. melanurus* and *C. picumnus*, as calculated in PopGenome. Averages for each species are indicated by dashed lines.

A model incorporating pulse migration and rate variation among loci was superior to simpler models, by Bayes factor (Supporting Information, Table S7). Assuming a migration pulse and a generation time of 2 years (see Material and Methods) yielded a species tree with a divergence between *C. picumnus* and *C. melanurus* of ~2.23 Mya (Table 1; Supporting Information, Table S6), whereas the divergence was ~1.71 years without a migration pulse (Table 1). Estimates of effective population sizes for Weipa and the remaining populations of *C. picumnus* ranged from ~601 000 and ~735 000, respectively; for the Pilbara population and remaining *C. melanurus* populations these values were ~162 000 and ~1.2 million, respectively (see Supporting Information, Table S6, for 95% CIs on all estimates). However, when generation times were assumed to be 5 years, as suggested by Bird *et al.* (2020), divergence times between the two species were ~4.3 and 5.6 Mya under among-locus variation, without and with pulse migration, respectively (Supporting Information, Table S6). There was a good correlation between the estimated rates for each locus estimated in bpp and the average nucleotide diversity of each locus across species as measured in PopGenome [Supporting Information, Fig. S10; $t = 4.567$, d.f. = 12, $P = 0.00064$, Pearson's rho = 0.797, 90% CI (0.5321, 0.919)].

Gene flow and hypothesis testing using migrate-n

For the within-species analyses, the best model within *C. picumnus* was one in which all five populations were designated and connected by unequal levels of gene flow between pairs in a linear-stepping stone (Table 2; Supporting Information, Table S9). This model had a model probability of 1 and was a better explanation of the data than models of two or one population. For *C. melanurus*, the best model (model probability 0.98) was one with four populations in which Newman was connected to Fitzroy Crossing, which was in turn connected to Doomadgee and Douglas Hot Springs in a triangle (Supporting Information, Table S8; Fig. S11).

We next analysed eight models involving both species and the entire set of populations, here considered as a single panmictic population, using both divergence with and without gene flow. We also considered an equilibrium migration model with unrestricted gene flow, again considering both species as single panmictic units (Supporting

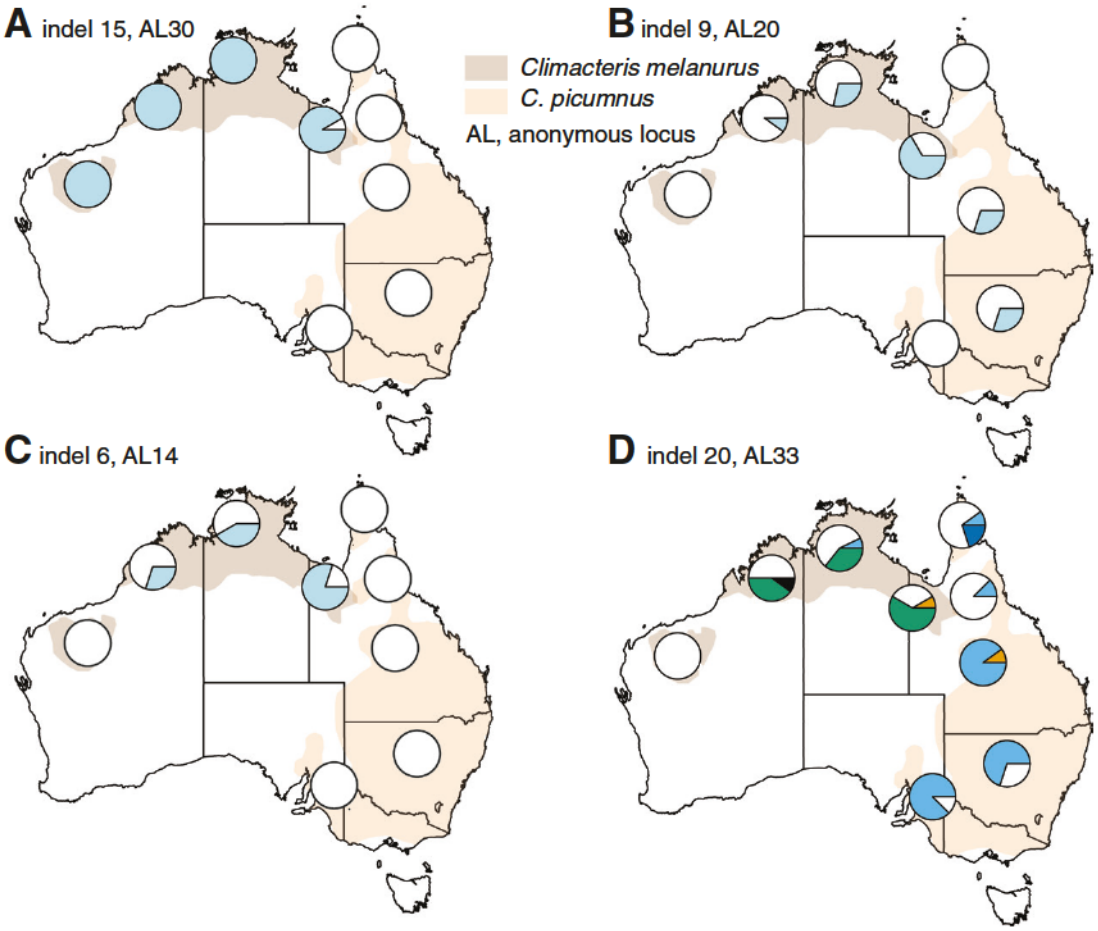

Figure 6. Examples of geographic variation of indels within *C. melanurus* and *C. picumnus*. Pie charts indicate the frequency of each indel variant for each of four example loci (A-D) that are polymorphic in one or both species. Details of indel variation can be found in Supporting Information, Table S5.

Information, Fig. S12). The two top models involving divergence between the two species (models 5 and 7) both also incorporated gene flow between the two species and had roughly equal likelihood (Supporting Information, Table S9). However, both of these models were outperformed by a simple equilibrium migration model between the two species, each panmictic, with no divergence component in the model (Supporting Information, Table S9). For models not including gene flow, and assuming a generation time of 2 years, the estimated divergence time between *C. picumnus* and *C. melanurus* was somewhat greater than inferred by bpp (~2.8 Mya with migrate-n vs. 1.7 Mya with bpp with among-locus rate variation; Table 2). The best isolation-migration model had an unrealistically large posterior mode and flat posterior distribution for divergence time (Supporting Information, Table S9). We therefore ran two additional isolation-migration models with an exponential instead of a flat prior on divergence time; these returned divergence times closer to those models without gene flow and to the migration-pulse model of bpp (posterior mode from prior mean divergence 0.001: 0.0047, or 4.7–5.5 Mya; Table 2, see Supporting Information, Table S8, for 95% CIs). The post hoc model with prior 0.001 had higher likelihood than even the equilibrium migration model.

Species distribution models and changes in effective population size through time

The niche models generated from GBIF records for *C. picumnus* ($N = 499$) and *C. melanurus* ($N = 243$) captured the major range blocks for both species (Fig. 7; Supporting Information, Figs S13–S14). Additionally, as expected, several regions not currently occupied by either species were predicted as suitable in the niche models. For example, for *C. picumnus*, a small region of south-west Western Australia was predicted to be suitable for current distribution with high probability, whereas for *C. melanurus*, the western half of Cape

Table 1. Summary of results of data analysis by Bayesian phylogenetics and phylogeography (bpp), assuming rate variation among loci. The left-hand column lists the current or ancestral population as designated in the Supporting Information, Figure S9. Φ_H and Φ_T indicate the probability of introgression into ancestral populations H and T, respectively. Parameter estimates assume a mutation rate of 2.2×10^{-9} substitutions per site per year and a generation time of 2 years. Results of additional runs are reported in Supporting Information, Table S6. n.e. = not estimated in the model.

		Parameter estimates (years or individuals)					
		Pure isolation model			Isolation-pulse migration		
Node in Supporting Information, Fig. S9	t or N_e	Mean	Lower	Upper	Mean	Lower	Upper
1	N_e	601 680	352 582	876 902	609 898	374 182	873 401
2	N_e	672 810	393 978	983 584	735 080	447 728	1 054 306
3	N_e	1 206 638	817 996	1 636 350	1 180 742	795 791	1 584 054
4	N_e	162 927	82 908	251 534	168 235	94 347	251 263
5	N_e	203 074	99 361	317 407	123 095	38 408	221 093
6	N_e	439 257	246 722	657 498	382 877	226 906	552 050
7	N_e	553 746	331 366	797 021	183 386	16 773	388 699
8	N_e	n.e.	n.e.	n.e.	477 569	295 288	679 554
9	N_e	n.e.	n.e.	n.e.	189 585	20 355	405 019
5	t	1 707 643	1 117 516	2 353 595	2 233 954	1 451 510	3 082 612
6	t	326 118	158 712	500 094	356 656	222 559	499 915
7	t	337 954	175 871	513 334	335 652	206 160	474 025
8	t	n.e.	n.e.	n.e.	343 617	212 118	484 846
9	t	n.e.	n.e.	n.e.	335 652	206 160	474 025
Φ_H	-	n.e.	n.e.	n.e.	0.065	0.016	0.122
Φ_T	-	n.e.	n.e.	n.e.	0.033	0.006	0.006

York Peninsula was predicted to be suitable with high probability. These same regions, as well as core regions of the current ranges, were predicted to be suitable during the Holocene and were included in regions of high long-term stability since the Pliocene (Fig. 7).

Areas of range overlap could influence the degree of gene flow and hence gene tree discordance observed in the DNA sequence data sets. We calculated the proportion of each species range that overlapped with ranges of other species for the 11 time periods investigated, from the Anthropocene to the mid-Pliocene (Fig. 8; Supporting Information, Fig. S15). We found that *C. picumnus and C. melanurus* overlapped at less than 10% of their range across these time periods, with the highest period of range overlap occurring in the Bølling-Allerød interstadial warming period during the Late Pleistocene (14.7–12.9 kya). The ranges of the two focal species also overlapped at various times in the past with outgroup species. For example, as much as 74% of the range of *C. picumnus* is predicted to have overlapped with that of *C. affinis* during the Late Holocene (4.2–0.3 kya), whereas about 62% of the range of *C. picumnus* overlaps with that of *C. affinis* today. The ranges of *C. picumnus* and the outgroup species *C. rufa* do not overlap today but were predicted to have overlapped substantially during the Late Pleistocene. The two outgroup species, *C. rufa* and *C. affinis*, are predicted to have overlapped in the past, with as much as 60% of the range of *C. rufa* overlapping with *C. affinis* during the mid-Pleistocene.

The total range areas of *C. picumnus* and *C. melanurus* were broadly similar across time periods, averaging 2 375 139 km² and 1 972 887 km², respectively. The range of *C. melanurus* fluctuated more widely over time (range: 1 299 250 to 3 175 545 km²) than the range of *C. picumnus* (range: 1 933 194 to 2 926 724 km²). However, the ranges of both species broadly declined over time, particularly during the since the Last Interglacial (~130 ka for *C. melanurus*) or Heinrich Stadial 1 (~15 ka) for *C. picumnus* (Fig. 8).

We analysed changes in effective population size over time using the Stairway method of Liu & Fu (2020) using both the unfolded (with outgroup polarization) and the folded (without outgroup polarization) SFSs. Although the unfolded SFS is likely more accurate, there is still uncertainty because the single outgroup allele we used to polarize mutations does not represent all the allelic variation in the outgroup; the folded SFS, although less informative than the unfolded SFS, is more robust in this regard.

Of the eight Stairway plots produced, all but one included a conspicuous drop in population size (Fig. 9;

Table 2. Summary of results of data analysis by migrate-n. Parameter estimates for the top three models- divergence, divergence with gene flow and equilibrium gene flow- are listed. Parameter estimates assume a mutation rate of 2.2×10^{-9} substitutions per site per year and a generation time of 2 years. Species 1 and 2 are *C. melanurus* and *C. picumnus*, respectively. *Ne* is effective population size, *Nm* is rate of gene flow, *D* is the divergence time and *S* is the standard deviation of the divergence time (Beerli *et al.*, 2022). Results of additional runs are reported in Supporting Information, Table S8

	No among-locus rate variation			Among-locus rate variation		
Parameter	**2.50%**	**Mean**	**97.5%**	**2.5%**	**Mean**	**97.5%**
Divergence without gene flow						
Ne_1	901 136	1 164 773	1 423 864	1 500 000	1 766 250	2 058 750
Ne_2	1 522 727	1 923 864	2 318 182	2 516 250	2 988 750	3 466 250
D_1->2	545 455	3 072 727	5 518 182	0	2 845 455	5 027 273
S_1->2	118 182	2 354 545	4 481 818	2 000 000	4 309 091	7 272 727
Divergence with gene flow						
Ne_1	742 045	996 591	1 242 045	1 250 000	1 454 545	1 644 318
Ne_2	1 386 364	1 775 000	2 151 136	2 386 364	2 880 682	3 371 591
Nm_2->1	0.00	0.86	3.35	0.14666663	1.177624576	2.21873329
Nm_1->2	0.00	1.42	5.68	0.42	2.456087985	4.7472
D_1->2	2 470 000	4 710 000	6 930 000	4 481 818	5 490 909	6 481 818
S_1->2	270 000	2 660 000	4 870 000	7 454 545	9 500 000	11 272 727
Equilibrium gene flow						
Ne_1	750 000	997 727	1 250 000	212 500	307 955	386 364
Ne_2	1 401 136	1 788 636	2 167 045	219 318	276 136	303 409
Nm_2->1	0.00	0.86	3.37	0.02493327	0.306792325	0.65733322
Nm_1->2	0.00	1.44	5.72	0	0.172663699	0.4272

Supporting Information, Tables S10 and S11); in the analysis of *C. melanurus* using the folded SFS from pegas, the decline was relatively mild. The onset of the decline in population size varied, from about 60–100 kya for the unfolded analyses across both species, to more recently (60–6 kya) for the folded analyses. In general, the plots reflected a pre-decline effective population size of ~1–1.2 million when using the unfolded SFS and ~300 000–800 000 when using the folded SFS. The post-decline populations closer to the present time varied around ~120 000–240 000 for the unfolded analyses and ~120 000–1 million for the folded analyses. All plots showed high uncertainty in overall effective population sizes, especially closer to the present and in several cases the 95% confidence limits could not exclude a constant population size throughout the tested periods (Fig. 9).

The effective population sizes from the Stairway plots using the folded PopGenome SFS or when accounting for ambiguous sites in the unfolded analyses were regressed against the estimated habitable area from the species distribution models (Supporting Information, Tables S11–S12). Effective population sizes from the Stairway plots were available for all time periods used in the species distribution models except for the most ancient period (Pliocene M2, ~3.3 Mya). There was also no available Stairway estimate of effective population size for the mid-Pliocene warm period (~3.2 Mya) for *C. picumnus* for the analyses using the pegas folded SFS. Linear models were fitted with both species together and separately. Of the six regressions performed (species pooled and separated for folded and unfolded analyses), effect sizes were generally small, with only the folded analysis for *C. picumnus* showing a significant relationship between effective population size through time and estimated habitable area (Supporting Information, Table S12).

DISCUSSION

We have used sequence variation among 14 anonymous nuclear loci and the mitochondrial CR1 to infer the phylogeographic history, patterns of natural selection and population growth, and extent of gene flow within and between a classic two-species complex of Australian treecreeper (*Climacteris*) displaying disjunct distributions across the Carpentarian barrier. Overall, our analyses documented substantial genetic differentiation within and between the two species in both mitochondrial and nuclear loci; the Pilbara population of *C. melanurus* was highly differentiated from those in the Top End, and the

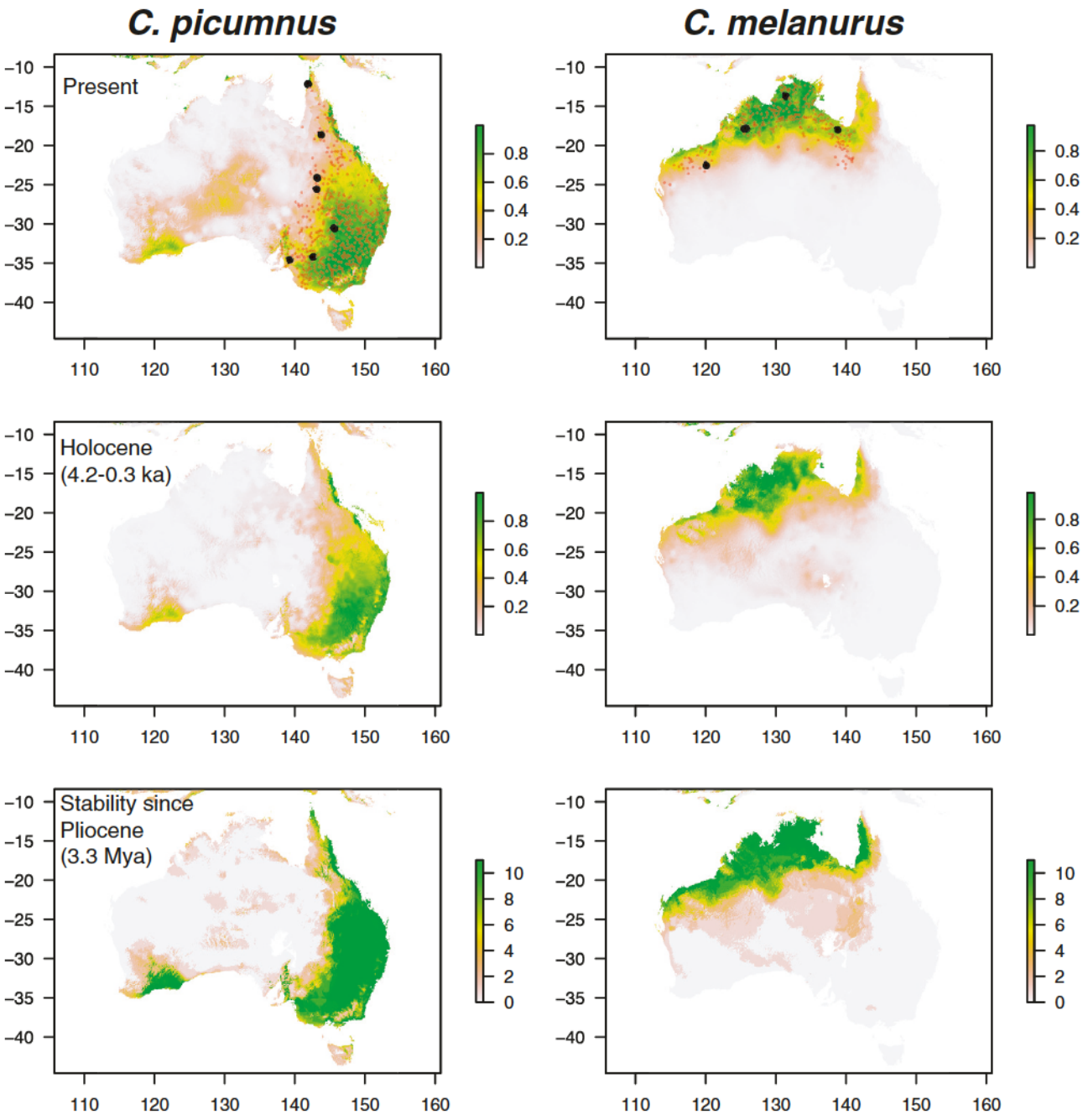

Figure 7. Environmental niche models of *C. picumnus* (left) and *C. melanurus* (right) for the present (top) and Holocene (middle) time periods. The niche stability since the Pliocene is depicted on the bottom row. In all panels, green indicates highest probability whereas brown and grey indicates lowest probability. *x*- and *y*-axes are longitude and latitude, respectively. Mya, millions of years ago; ka, thousands of years ago.

Cape York Peninsula population of *C. picumnus* (*melanotus*) is somewhat less strongly differentiated from more southerly populations. Both of these patterns corroborate putative subspecies boundaries (Keast, 1957; Ford, 1987), but we cannot rule out an isolation-by-distance model for differentiation of *C. p. melanotus*. *Climacteris picumnus* and *C. melanurus* are substantially differentiated from each other across the Carpentarian barrier, although Bayesian analyses detected a low level of gene flow across this barrier. Depending on the value of generation time assumed, *C. picumnus* and *C. melanurus* could have diverged as long ago as 5.58 Mya [95% CI (3.86–7.43), Supporting Information, Table S6]. In general, our analyses

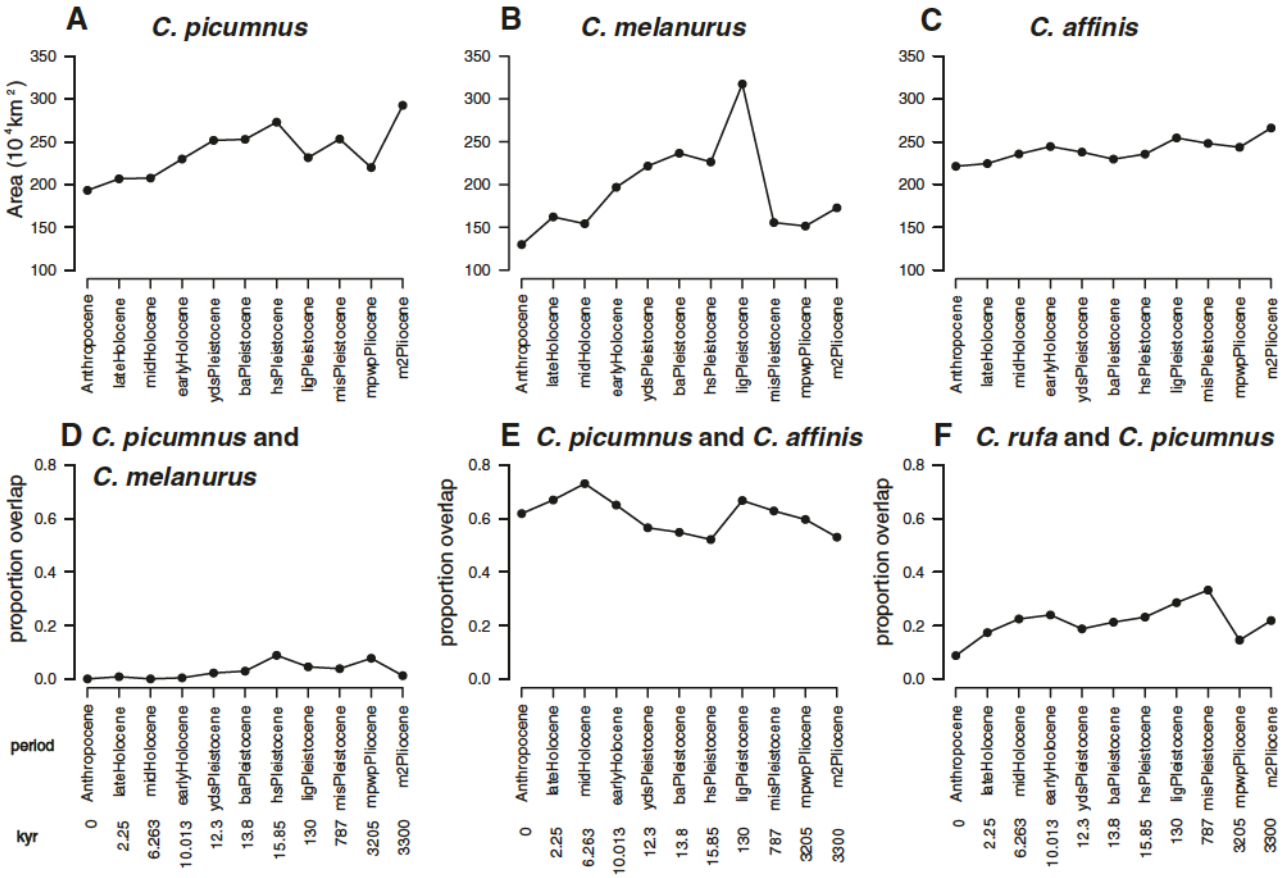

Figure 8. Estimated ranges and proportion of range overlap of *C. melanurus* and *C. picumnus*, through 11 time periods from the mid-Pliocene to the present (Anthropocene). A-C, changes in estimated range size over time for *C. picumnus* (A), *C. melanurus* (B) and outgroup species *C. affinis* (C). D-F, proportion of range overlap over time for *C. picumnus*-*C. melanurus* (D), *C. picumnus*-*C. affinis* (E) and outgroup species *C. rufa* and *C. picumnus* (F). For (D-F), the proportion of the range of the first species listed is indicated on the *y*-axis. Additional details can be found in Supporting Information, Figs S11–S12.

showed higher nucleotide diversity among autosomal nuclear markers than for the mtDNA control region, which showed evidence of directional selection (negative Tajima's *D*) at the microevolutionary level. Analyses of population size changes through time consistently showed declines in effective population size since the Holocene or Late Pleistocene, depending on the analysis. Although estimated palaeospecies distribution models also showed declines in habitable range since the Late Pleistocene (~15–130 ka), the correlation with effective population size was weak. Overall, *C. picumnus* and *C. melanurus* exhibit patterns expected for differentiation across the Carpentarian and associated barriers, although additional complexity in terms of gene flow and reticulation suggests a dynamic relationship with the evolving landscape of the northern Australian Monsoon Tropics seen in birds and other vertebrates (Bowman *et al.*, 2010; Fujita *et al.*, 2010; Potter *et al.*, 2012, 2018; Dorrington *et al.*, 2020; Burley *et al.*, 2022).

Natural selection on mtDNA in *C. picumnus*

An important goal of the mitochondrial survey was to determine if signals of natural selection detected by Lamb *et al.* (2018) were evident in the mtDNA control region. Importantly, the mitochondrial sequencing and analysis for this project took place prior to the publication of Lamb *et al.* (2018), yet the two studies converged on similar conclusions. Lamb *et al.* (2018) conducted a variety of macroevolutionary tests for natural selection in the mitogenome of treecreepers and other Australian birds, and found that sequence within species varied with climate features in ways that suggested adaptation. However, they did not conduct any formal tests of selection within species: statistical tests of natural selection were confined to understanding patterns of amino acid substitution across the mitogenome tree of the multiple species studied. We examined nucleotide diversity and Tajima's *D* within both *C. picumnus* and *C. melanurus*. We found surprisingly low levels of nucleotide diversity (π) within *C. picumnus* (Fig. 2): in

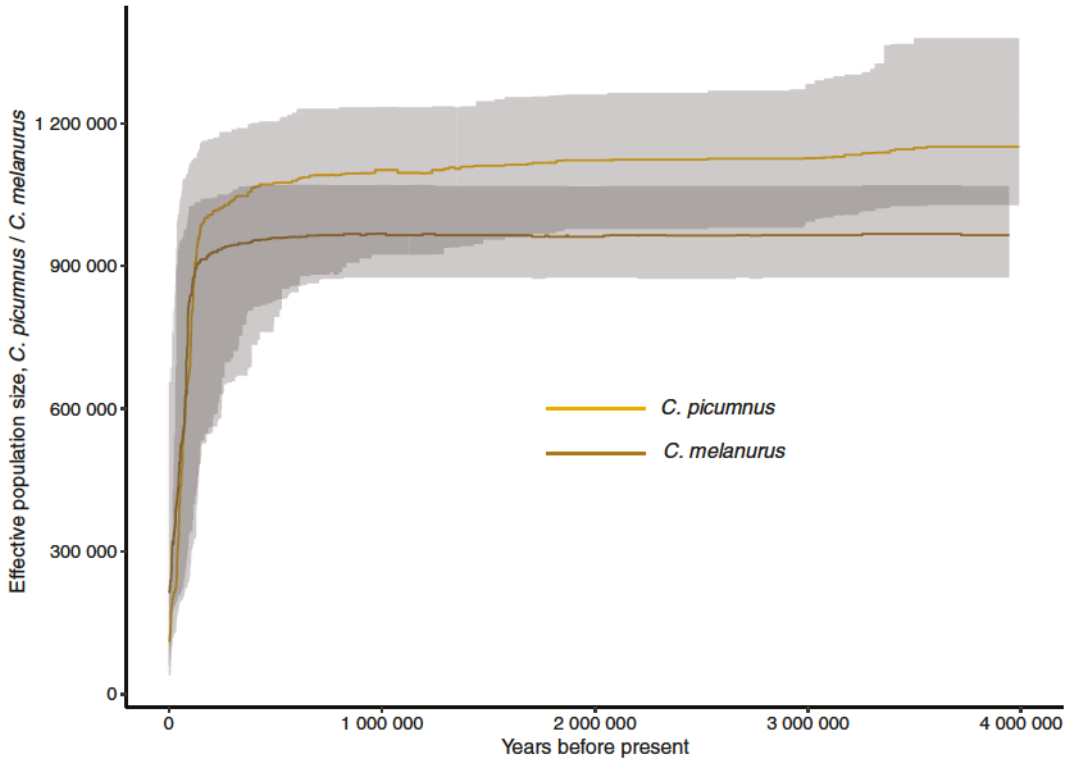

Figure 9. Effective population size through time for *C. melanurus* and *picumnus* as estimated by the Stairway method. The *x*-axis shows times from ~3 Mya to the present, assuming a substitution rate of 2.2×10^{-9} substitutions per site per year and a generation time of 2 year. Light brown, *C. picumnus*, dark brown, *C. melanurus*. Ninety-five percent confidence limits on the estimates are shown in grey and their overlap in darker light grey.

all but one population (Weipa) mtDNA diversity was lower than in the nuclear genome. Although this pattern alone is not inconsistent with neutrality at mtDNA, it is unusual: nucleotide diversity in birds is systematically lower than in mammals and is thought to be depressed due to effective linkage and hitchhiking with the W chromosome, which is subject to Hill–Robertson effects (Berlin *et al.*, 2007). The extent to which mitochondrial nucleotide diversity in animals varies with effective population size, as predicted for a neutral chromosome, or whether it is subject to pervasive natural selection, which obliterates the correlation of nucleotide diversity and *Ne*, is controversial (Bazin *et al.*, 2006; Allio *et al.*, 2017). Recent analyses confirm that the mutation rate of mtDNA is substantially higher than that for the nuclear genome in birds (Wilson *et al.*, 1985; Allio *et al.*, 2017), and that uncorrected percent divergence for mtDNA is in general higher within species than for nuclear DNA—presumably driven by the higher mitochondrial mutation rate (Bazin *et al.*, 2006; Allio *et al.*, 2017). Thus, the uniformly lower mtDNA diversity in *Climacteris* treecreepers could be an indirect indication of the action of diversity-reducing selective sweeps.

We also found that Tajima's *D* for the mtDNA CR1 was strongly negative in *C. picumnus*, potentially suggesting a recent selective sweep. Tajima's *D* was not significantly negative for *C. melanurus*, but was strongly negative for two nuclear loci in *C. melanurus* and one nuclear locus in *C. picumnus* (Fig. 5). This pattern is particularly noteworthy given that the overall population trajectory in both species was one of decline over time, which should yield positive rather than negative values of D. These results provide an additional line of evidence implicating natural selection in the pattern of mitochondrial diversity in *C. picumnus*, potentially in response to environmental or climatic gradients (Lamb *et al.*, 2018).

Phylogeographic and population genetic patterns

Brown and black-tailed treecreepers exhibit many of the patterns expected for species complexes diverging by allopatric speciation across the Carpentarian barrier (reviewed in Cracraft, 1986; Edwards, 1993; Lee & Edwards, 2008; Joseph & Omland, 2009; Edwards *et al.*, 2013; Kearns *et al.*, 2014; Joseph *et al.*, 2019; Peñalba *et al.*, 2019; Burley *et al.*, 2022). The F_{st} for both mitochondrial and nuclear DNA was highest between treecreeper species across the Carpentarian

and between lesser barriers separating subspecies, such as the Black Mountain Corridor separating Cape York Peninsula and more southerly populations in the east, and the Canning Divide/ Great Sandy Desert separating the Pilbara from regions further north in the west (Fig. 1: Pepper *et al.*, 2013b; Edwards *et al.*, 2017). Consistent with classical work, differentiation of *C. melanurus* across the Ord Arid Intrusion separating the Kimberley from the Top End was mild (Ford, 1978), but more pronounced for *C. picumnus* populations separated by the Einasleigh uplands and the Burdekin-Lynd Divide and associated highlands (Ford, 1986). For birds, the Pilbara is still poorly studied in terms of genetic diversity and divergence from other Top End populations (Edwards, 1993; Lee & Edwards, 2008; Pepper *et al.*, 2013b; Black *et al.*, 2020), although additional work has been produced for other vertebrate groups (Pepper *et al.*, 2006; Melville *et al.*, 2016; Potter *et al.*, 2019; Umbrello *et al.*, 2020). A relatively small number of avian subspecies are endemic to the Pilbara, but genetic analysis of additional groups may reveal others (Johnstone *et al.*, 2013; Dorrington *et al.*, 2020; Joseph *et al.*, 2020).

We found lower genetic diversity in the Pilbara *C. melanurus*, as well as in the Sedan sample in *C. picumnus*. Although our sample size was somewhat low for the Pilbara ($N = 4$ individuals) the number of alleles we sampled was adequate for estimating genetic diversity (Felsenstein, 2006). Our MIGRATE analyses largely corroborated these results: a modified two-population model (with Pilbara distinct) was favoured for *C. melanurus* and a five-population model with subtle and more widespread differentiation was favoured for *C. picumnus*. The genetic isolation of the Pilbara, and Sedan to a lesser extent, likely has facilitated a pattern seen in the blue-faced honeyeater (*Entomyzon cyanotis*) in which terminal and peripheral populations harbour less diversity (Burley *et al.*, 2022).

Our analysis of noncoding loci in treecreepers allowed us to examine indel variation within and among loci and populations. We found that the F_{st} for indels among populations was slightly higher than for SNPs. This result could mean that low levels of diversifying selection act on indels to a greater extent than SNPs in our data set, perhaps due to effects on gene regulation. In animals, indels have not been examined extensively in studies of geographic variation of nuclear genes of birds or other groups (Brito & Edwards, 2009), although they have been important in phylogenetic reconstruction (Douglas *et al.*, 2010; Lee *et al.*, 2012; Houde *et al.*, 2019). Schaeffer (2002) examined indel diversity among multiple strains of *Drosophila pseudoobscura*, modelled as a single population, and found that purifying selection acted on deletion variants but not insertion variants. Indels, including microsatellites, can have measurable effects on gene expression (Rockman & Wray, 2002; Gagliano *et al.*, 2019) and deserve further study in the context of phylogeography.

Multiple analyses suggested the presence of gene flow between *C. picumnus* and *C. melanurus*. Coalescent simulations as well as Phrapl suggested that divergence followed by gene flow was a better explanation of the data than a pure divergence without gene flow model. A pure isolation model in bpp yielded estimates of divergence times of 1.7 Mya (95% CI 1.2–2.4 Mya) when rate variation among loci was assumed (Table 1). By contrast, when using migrate-n, an equilibrium migration model with asymmetrical gene flow between the two species outcompeted eight divergence models with and without gene flow. When we conducted post hoc analyses of two additional isolation-migration models with different priors on divergence time, one of these models outperformed even the equilibrium migration model. Clearly the signal in the data for divergence time is not strong because the posterior distribution in this model is influenced by the prior, highlighting the challenges of estimating parameters of a true isolation-migration model, as opposed to the migration-pulse model of bpp (Flouri *et al.*, 2020; Beerli *et al.*, 2022). However, our analysis and data at this point cannot distinguish between these models, both of which are likely simplifications of the true process. Nonetheless, across all analyses, the level of gene flow estimated between the two species was low: bpp indicated low probabilities of introgression (Table 1) and by estimated migrate-n *Nm* was 0.84 migrants per generation from *C. picumnus* to *C. melanurus* and 1.4 migrants per generation in the opposite direction (Table 2). *C. picumnus* and *C. melanurus* are quite phenotypically distinct, and their population density in any putative region of intergradation is very low. The ecological niche models suggested that the area of putative regions of range overlap between *C. picumnus* and *C. melanurus* has been very low throughout the past several million years, peaking at less than 10% at about 13 000 years ago. Thus, the opportunities for gene flow between the species appear small. Peñalba *et al.* (2019) found a decrease in probability of gene flow in this region between populations diverging at the level of autosomal F_{st} of 0.3–0.4, corresponding roughly to mitochondrial divergences of ~1.1–1.7 Mya. The treecreeper mitochondrial data suggest the F_{st} between *C. picumnus* and *C. melanurus* is much greater than 0.4 and autosomal divergence times closer to 2 Mya across bpp (with gene flow) and migrate-n (without gene flow). Use of a 5-year generation time greatly increases our estimated divergence times to dates often in the Miocene and earlier; such ancient divergence times have not yet been observed for birds or other vertebrates for the Carpentarian barrier (Kearns *et al.*, 2014; Edwards *et al.*, 2016; Peñalba *et al.*, 2017, 2019; Dorrington *et al.*, 2020), although they are known for other biomes in Australia (Mitchell *et al.*, 2021).

The peak overlaps in geographic range between ingroup and outgroup species pairs in our data set, such as *C. rufa* - *C. picumnus* (> 30% range overlap), and especially *C. rufa* - *C. affinis* (> 60% overlap) and *C. picumnus* and *C. affinis* (> 70%) suggest the possibility of past sympatric interactions such as gene flow in this clade more so than possible for *C. picumnus* and *C. melanurus*. In addition to incomplete lineage sorting, such geographic overlap facilitating hybridization could explain some of the instances of excessive lineage sharing and lack of reciprocal monophyly observed in the gene trees, involving not just sister species but all species in the study. Extensive lineage sharing at nuclear loci is common for Australian birds, yet we know little about the extent of geographic range overlap in the past (Joseph & Omland, 2009; Lee *et al.*, 2012). Analyses such as ours could help clarify the sources of lineage sharing in nuclear and mitochondrial gene trees in Australian birds.

Distribution models and effective population sizes through time

The relationship between population size changes through time and historically available niche area is of ongoing interest in molecular ecology (Miller *et al.* 2021). Although our data set was not genome wide and was modest in size, the Stairway plots consistently suggested a general reduction in the effective population size of both *C. picumnus* and *C. melanurus* since the Late Pliocene. Depending on the details of the models, this reduction either occurred abruptly around 10 000 years ago, or, more likely, based on the unfolded SFS analyses, more gradually over time. We found that the estimated area of range overlap of suitable habitat between *C. picumnus* and *C. melanurus* also declined through time, more recently for *C. picumnus* than for *C. melanurus*. Overall, however, we found little correlation between estimates of effective population size through time for either species and predicted areas of suitable habitat, perhaps because both parameters are challenging to estimate. Still, our distribution models will be important starting points for more detailed analyses with genome-wide data sets in the future.

In summary, our analyses of a modest data set of nuclear and mitochondrial sequence-based markers have clarified numerous aspects of the phylogeography, population history and potential for natural selection in brown and black-tailed treecreepers. In the future, integration of phenotypic analyses, facilitated by the freely available voucher specimens made for this study, and genome-wide analyses will provide additional insight into the genetic basis of phenotypic divergence and its interactions with population history. For example, genome-wide data would allow measurement of differential gene flow across regions of the genome, identification of genomic islands of natural selection, and would perhaps allow us to distinguish between various models of gene flow over time encompassed by our analyses (Turner & Hahn, 2010; Cruickshank & Hahn, 2014; Edwards *et al.*, 2015). Our efforts are currently directed towards this end.

ACKNOWLEDGEMENTS

All specimens were collected between 1996 and 2002 under the appropriate permits in New South Wales, Queensland, Northern Territory and Western Australia. We thank Christopher Hess, Peter Gagne, Anne Hilborn, Monica Silva, Catherine Smith, Sievert Rohwer, Walter Boles and Wayne Longmore for assistance collecting specimens in the field. Angus and Karen Emmott graciously allowed access to Noonbah Station, as did the owners of Roy Hill Station, Western Australia. We thank the Indigenous communities at Doomadgee and Leopold Downs for access to their land. We thank Sharon Birks and the staff of the Ornithology Department at the University of Washington Burke Museum of Natural History and Culture for facilitating loans of tissues used in this study. We thank Bastien Pfeifer for advice on PopGenome, Emmanuel Paradis for clarification of ape and pegas functions, and Tomáš Flouri and Ziheng Yang for assistance with bpp. We thank Michael Whitlock and Stephen Garnett for helpful discussion, Robert Boria, Rus Hoelzel and Leo Joseph for very helpful comments on an earlier draft of this paper, and three anonymous reviewers for comments on the original submitted version. Thanks to Graeme Chapman for providing photos of *C. picumnus* and *C. melanurus* for use in Figure 1. Computation for this paper was conducted on the Harvard University Cannon Computing Cluster and the Florida State University computing cluster. This work was funded by National Science Foundation (NSF) grant DEB-0500862 to S.V.E. and NSF grants DBI-1145999, DBI-1564822 and DBI-2019989 to P.B. J.F.R.T. acknowledges support from the Lemann Foundation, the David Rockefeller Center for Latin American Studies at Harvard University, the Harvard University Global Climate Fund and NSF DEB-1949749. The authors have no conflicts of interest to declare. We thank the Wetmore Colles Fund of the Museum of Compatative Zoology for partially covering page and open access charges of this paper.

DATA AVAILABILITY

The sequence data have been submitted to GenBank under accession numbers OP498356-OP499811. Data sets associated with this paper, including environmental niche modelling, Bayesian analyses of population structure and scripts have been deposited in the Dryad digital repository (Edwards *et al.*, 2022).

REFERENCES

Allio R, Donega S, Galtier N, Nabholz B. 2017. Large variation in the ratio of mitochondrial to nuclear mutation rate across animals: implications for genetic diversity and the use of mitochondrial DNA as a molecular marker. *Molecular Biology and Evolution* **34**: 2762–2772.

Angelis K, dos Reis M. 2015. The impact of ancestral population size and incomplete lineage sorting on Bayesian estimation of species divergence times. *Current Zoology* **61**: 874–885.

Bakker VJ, Finkelstein ME, D'Elia J, Doak DF, Kirkland S. 2022. Genetically based demographic reconstructions require careful consideration of generation time. *Current Biology* **32**: R356–R357.

Balakrishnan CN, Lee JY, Edwards SV. 2010. Phylogeography and phylogenetics in the nuclear age. In: Grant P, Grant R, eds. *Searching for the causes of evolution: from field observations to mechanisms*. Princeton: Princeton University Press, 65–88.

Bazin E, Glémin S, Galtier N. 2006. Population size does not influence mitochondrial genetic diversity in animals. *Science* **312**: 570–572.

Beerli P. 2006. Comparison of Bayesian and maximum likelihood inference of population genetic parameters. *Bioinformatics* **22**: 341–345.

Beerli P, Ashki H, Mashayekhi S, Palczewski M. 2022. Population divergence time estimation using individual lineage label switching. *G3 Genes|Genomes|Genetics* **12**: jkac040.

Beerli P, Felsenstein J. 1999. Maximum-likelihood estimation of migration rates and effective population numbers in two populations using a coalescent approach. *Genetics* **152**: 763–773.

Beerli P, Palczewski M. 2010. Unified framework to evaluate panmixia and migration direction among multiple sampling locations. *Genetics* **185**: 313–326.

Beier S, Thiel T, Münch T, Scholz U, Mascher M. 2017. MISA-web: a web server for microsatellite prediction. *Bioinformatics* **33**: 2583–2585.

Bennett VA, Doerr VAJ, Doerr ED, Manning AD, Lindenmayer DB. 2012a. The anatomy of a failed reintroduction: a case study with the brown treecreeper. *Emu - Austral Ornithology* **112**: 298–312.

Bennett VA, Doerr VAJ, Doerr ED, Manning AD, Lindenmayer DB, Yoon HJ. 2012b. Habitat selection and post-release movement of reintroduced brown treecreeper individuals in restored temperate woodland. *PLoS One* **7**: e50612.

Berlin S, Tomaras D, Charlesworth B. 2007. Low mitochondrial variability in birds may indicate Hill–Robertson effects on the W chromosome. *Heredity* **99**: 389–396.

Bertrand JAM, Bourgeois YXC, Delahaie B, Duval T, García-Jiménez R, Cornuault J, Heeb P, Milá B, Pujol B, Thébaud C. 2014. Extremely reduced dispersal and gene flow in an island bird. *Heredity* **112**: 190–196.

Bird JP, Martin R, Akçakaya HR, Gilroy J, Burfield IJ, Garnett ST, Symes A, Taylor J, Şekercioğlu CH, Butchart SHM. 2020. Generation lengths of the world's birds and their implications for extinction risk. *Conservation Biology* **34**: 1252–1261.

Black AB, Wilson CA, Pedler LP, McGregor SR, Joseph L. 2020. Two new but threatened subspecies of rufous grasswren *Amytornis whitei* (Maluridae). *Bulletin of the British Ornithologists' Club* **140**: 151–163.

Bowman DM, Brown G, Braby M, Brown J, Cook LG, Crisp M, Ford F, Haberle S, Hughes J, Isagi Y. 2010. Biogeography of the Australian monsoon tropics. *Journal of Biogeography* **37**: 201–216.

Brito PH, Edwards SV. 2009. Multilocus phylogeography and phylogenetics using sequence-based markers. *Genetica* **135**: 439–455.

Brown JL, Hill DJ, Dolan AM, Carnaval AC, Haywood AM. 2018. PaleoClim, high spatial resolution paleoclimate surfaces for global land areas. *Scientific Data* **5**: 180254.

Bryant LM, Krosch MN. 2016. Lines in the land: a review of evidence for eastern Australia's major biogeographical barriers to closed forest taxa. *Biological Journal of the Linnean Society* **119**: 238–264.

Burley JT, Orzechowski SCM, Sin SYW, Edwards SV. 2022. Whole-genome phylogeography of the blue-faced honeyeater (*Entomyzon cyanotis*) and discovery and characterization of a neo-Z chromosome. *Molecular Ecology* **00**:1–23. https://doi.org/10.1111/mec.16604.

Caetano DS, Quental TB. 2022. How important is budding speciation for comparative studies? *bioRxiv*, doi: 10.1101/2022.05.24.493296, 25 May 2022, preprint: not peer reviewed.

Carstens BC, Morales AE, Jackson ND, O'Meara BC. 2017. Objective choice of phylogeographic models. *Molecular Phylogenetics and Evolution* **116**: 136–140.

Catullo RA, Lanfear R, Doughty P, Keogh JS. 2014. The biogeographical boundaries of northern Australia: evidence from ecological niche models and a multi-locus phylogeny of *Uperoleia* toadlets (Anura: Myobatrachidae). *Journal of Biogeography* **41**: 659–672.

Chamberlain S, Barve V, Mcglinn D, Oldoni D, Desmet P, Geffert L, Ram K. 2021. *rgbif: Interface to the Global Biodiversity Information Facility API*. https://CRAN.R-project.org/package=rgbif

Cracraft J. 1986. Origin and evolution of continental biotas: speciation and historical congruence within the Australian avifauna. *Evolution* **40**: 977–996.

Cruickshank TE, Hahn MW. 2014. Reanalysis suggests that genomic islands of speciation are due to reduced diversity, not reduced gene flow. *Molecular Ecology* **23**: 3133–3157.

Doerr ED, Doerr VAJ. 2006. Comparative demography of treecreepers: evaluating hypotheses for the evolution and maintenance of cooperative breeding. *Animal Behaviour* **72**: 147–159.

Doerr ED, Doerr VAJ. 2007. Positive effects of helpers on reproductive success in the brown treecreeper and the general importance of future benefits. *Journal of Animal Ecology* **76**: 966–976.

Dorrington A, Joseph L, Hallgren W, Mason I, Drew A, Hughes JM, Schmidt DJ. 2020. Phylogeography of the blue-winged kookaburra *Dacelo leachii* across tropical northern Australia and New Guinea. *Emu - Austral Ornithology* **120**: 33–45.

Doughty P, Bourke G, Tedeschi LG, Pratt RC, Oliver PM, Palmer RA, Moritz C. 2018. Species delimitation in

the *Gehyra nana* (Squamata: Gekkonidae) complex: cryptic and divergent morphological evolution in the Australian Monsoonal Tropics, with the description of four new species. *Zootaxa* **4403**: 201–244.

Doughty P, Rolfe JK, Burbidge AH, Pearson DJ, Kendrick PG. 2011. Herpetological assemblages of the Pilbara biogeographic region, Western Australia: ecological associations, biogeographic patterns and conservation. *Records of the Western Australian Museum Supplement* **78**: 315–341.

Douglas ME, Douglas MR, Schuett GW, Beck DD, Sullivan BK. 2010. Conservation phylogenetics of helodermatid lizards using multiple molecular markers and a supertree approach. *Molecular Phylogenetics and Evolution* **55**: 153–167.

Earl DA, vonHoldt BM. 2012. STRUCTURE HARVESTER: a website and program for visualizing STRUCTURE output and implementing the Evanno method. *Conservation Genetics Resources* **4**: 359–361.

Edwards RD, Crisp MD, Cook DH, Cook LG. 2017. Congruent biogeographical disjunctions at a continent-wide scale: quantifying and clarifying the role of biogeographic barriers in the Australian Tropics. *PLoS One* **12**: e0174812.

Edwards RD, Crisp MD, Cook LG. 2013. Niche differentiation and spatial partitioning in the evolution of two Australian monsoon tropical tree species. *Journal of Biogeography* **40**: 559–569.

Edwards SV. 1993. Long-distance gene flow in a cooperative breeder detected in genealogies of mitochondrial DNA sequences. *Proceedings of the Royal Society of London Series B* **252**: 177–185.

Edwards SV, Potter S, Schmitt CJ, Bragg JG, Moritz C. 2016. Reticulation, divergence, and the phylogeography-phylogenetics continuum. *Proceedings of the National Academy of Sciences* **113**: 8025–8032.

Edwards SV, Robin VV, Ferrand N, Moritz C. 2021. The evolution of comparative phylogeography: putting the geography (and more) into comparative population genomics. *Genome Biology and Evolution* **14**: evab176.

Edwards SV, Shultz AJ, Campbell-Staton SC. 2015. Next-generation sequencing and the expanding domain of phylogeography. *Folia Zoologica* **64**: 187–206.

Edwards SV, Tonini JFR, McInerney N, Welch C, Beerli P. 2022. Multilocus phylogeography, population genetics and niche evolution of Australian brown and black-tailed treecreepers (Aves: Climacteris). *Dryad Dataset*, https://doi.org/10.5061/dryad.bcc2fqzgt

Eldridge MDB, Potter S, Cooper SJB. 2012. Biogeographic barriers in north-western Australia: an overview and standardisation of nomenclature. *Australian Journal of Zoology* **59**: 270–272.

Evanno G, Regnaut S, Goudet J. 2005. Detecting the number of clusters of individuals using the software STRUCTURE: a simulation study. *Molecular Ecology* **14**: 2611–2620.

Ewart KM, Lo N, Ogden R, Joseph L, Ho SYW, Frankham GJ, Eldridge MDB, Schodde R, Johnson RN. 2020. Phylogeography of the iconic Australian red-tailed black-cockatoo (*Calyptorhynchus banksii*) and implications for its conservation. *Heredity* **125**: 85–100.

Fay JC, Wyckoff GJ, Wu CI. 2001. Positive and negative selection on the human genome. *Genetics* **158**: 1227–1234.

Felsenstein J. 1994. *Phylogeny Inference Package (PHYLIP), version 3.6*. Seattle: University of Washington.

Felsenstein J. 2006. Accuracy of coalescent likelihood estimates: do we need more sites, more sequences, or more loci? *Molecular Biology and Evolution* **23**: 691–700.

Fitch WM. 1971. Toward defining the course of evolution: minimum change for a specific tree topology. *Systematic Zoology* **20**: 406–416.

Flores-Rentería L, Rymer PD, Ramadoss N, Riegler M. 2021. Major biogeographic barriers in eastern Australia have shaped the population structure of widely distributed *Eucalyptus moluccana* and its putative subspecies. *Ecology and Evolution* **11**: 14828–14842.

Flouri T, Jiao X, Rannala B, Yang Z. 2018. Species tree inference with BPP using genomic sequences and the multispecies coalescent. *Molecular Biology and Evolution* **35**: 2585–2593.

Flouri T, Jiao X, Rannala B, Yang Z. 2020. A Bayesian implementation of the multispecies coalescent model with introgression for phylogenomic analysis. *Molecular Biology and Evolution* **37**: 1211–1223.

Ford HA, Walters JR, Cooper CB, Debus SJS, Doerr VAJ. 2009. Extinction debt or habitat change? Ongoing losses of woodland birds in north-eastern New South Wales, Australia. *Biological Conservation* **142**: 3182–3190.

Ford J. 1978. Geographical isolation and morphological and habitat differentiation between birds of the Kimberley and Northern Territory. *Emu - Austral Ornithology* **78**: 25–35.

Ford J. 1986. Hybridization and allopatry in the region of the Einasleigh Uplands and Burdekin-Lynd Divide, north-eastern Queensland. *Emu - Austral Ornithology* **86**: 87–110.

Ford J. 1987. Minor isolates and minor geographical barriers in avian speciation in continental Australia. *Emu - Austral Ornithology* **87**: 90–102.

Fujita MK, McGuire JA, Donnellan SC, Moritz C. 2010. Diversification and persistence at the arid-monsoonal interface: Australia-wide biogeography of the Bynoe's gecko (*Heteronotia binoei*; Gekkonidae). *Evolution* **64**: 2293–2314.

Gagliano SA, Sengupta S, Sidore C, Maschio A, Cucca F, Schlessinger D, Abecasis GR. 2019. Relative impact of indels versus SNPs on complex disease. *Genetic Epidemiology* **43**: 112–117.

Goudet J. 2005. hierfstat, a package for R to compute and test hierarchical F-statistics. *Molecular Ecology Notes* **5**: 184–186.

Hancock AM, Rienzo AD. 2008. Detecting the genetic signature of natural selection in human populations: models, methods, and data. *Annual Review of Anthropology* **37**: 197–217.

Hare MP, Avise JC. 1998. Population structure in the American oyster as inferred by nuclear gene genealogies. *Molecular Biology and Evolution* **15**: 119–128.

Hare MP, Karl SA, Avise JC. 1996. Anonymous nuclear DNA markers in the American oyster and their implications for

the heterozygote deficiency phenomenon in marine bivalves. *Molecular Biology and Evolution* **13**: 334–345.

Hey J, Machado CA. 2003. The study of structured populations - new hope for a difficult and divided science. *Nature Reviews Genetics* **4**: 535–543.

Hey J, Nielsen R. 2004. Multilocus methods for estimating population sizes, migration rates and divergence time, with applications to the divergence of *Drosophila pseudoobscura* and *D. persimilis*. *Genetics* **167**: 747–760.

Hijmans RJ, Phillips S, Leathwick J, Elith J. 2011. *dismo: species distribution modeling v.0.6-3*. Available at: http://cran.r-project.org/web/packages/dismo/

Houde P, Braun EL, Narula N, Minjares U, Mirarab S. 2019. Phylogenetic signal of indels and the neoavian radiation. *Diversity* **11**: 108. https://doi.org/10.3390/d11070108.

Hudson RR. 2002. Generating samples under a Wright–Fisher neutral model of genetic variation. *Bioinformatics* **18**: 337–338.

Hudson RR, Slatkin M, Maddison WP. 1992. Estimation of levels of gene flow from DNA sequence data. *Genetics* **132**: 583–589.

Jackson ND, Morales AE, Carstens BC, O'Meara BC. 2017. PHRAPL: Phylogeographic Inference Using Approximate Likelihoods. *Systematic Biology* **66**: 1045–1053.

Jennings WB, Edwards SV. 2005. Speciational history of Australian grass finches (*Poephila*) inferred from 30 gene trees. *Evolution* **59**: 2033–2047.

Johnstone RE, Burbidge AH, Darnell JC. 2013. Birds of the Pilbara region, including seas and offshore islands, Western Australia: distribution, status and historical changes. *Records of the Western Australian Museum Supplement* **78**: 343–411.

Jonasson J, Harkonen T, Sundqvist L, Edwards SV, Harding KC. 2022. A unifying framework for estimating generation time in age-structured populations: implications for phylogenetics and conservation biology. *The American Naturalist* **200**: 48–62.

Joseph L, Bishop KD, Wilson CA, Edwards SV, Iova B, Campbell CD, Mason I, Drew A. 2019. A review of evolutionary research on birds of the New Guinean savannas and closely associated habitats of riparian rainforests, mangroves and grasslands. *Emu - Austral Ornithology* **119**: 317–330.

Joseph L, Omland KE. 2009. Phylogeography: its development and impact in Australo-Papuan ornithology with special reference to paraphyly in Australian birds. *Emu - Austral Ornithology* **109**: 1–23.

Kalyaanamoorthy S, Minh BQ, Wong TKF, von Haeseler A, Jermiin LS. 2017. ModelFinder: fast model selection for accurate phylogenetic estimates. *Nature Methods* **14**: 587–589.

Kang Y-J, Yang D-C, Kong L, Hou M, Meng Y-Q, Wei L, Gao G. 2017. CPC2: a fast and accurate coding potential calculator based on sequence intrinsic features. *Nucleic Acids Research* **45**: W12–W16.

Kearns AM, Joseph L, Toon A, Cook LG. 2014. Australia's arid-adapted butcherbirds experienced range expansions during Pleistocene glacial maxima. *Nature Communications* **5**: 3994.

Keast A. 1957. Variation and speciation in the genus *Climacteris* Temminck (Aves: Sittidae). *Australian Journal of Zoology* **5**: 474–495.

Keast, A. 1961. Bird speciation on the Australian Continent. *Bulletin of the Museum of Comparative Zoology* **123**: 303–495.

Knowles LL, Carstens BC, Keat ML. 2007. Coupling genetic and ecological-niche models to examine how past population distributions contribute to divergence. *Current Biology* **17**: 940–946.

Lamb AM, Gan HM, Greening C, Joseph L, Lee Yin P, Morán-Ordóñez A, Sunnucks P, Pavlova A. 2018. Climate-driven mitochondrial selection: a test in Australian songbirds. *Molecular Ecology* **27**: 898–918.

Lamb AM, Gonçalves da Silva A, Joseph L, Sunnucks P, Pavlova A. 2019. Pleistocene-dated biogeographic barriers drove divergence within the Australo-Papuan region in a sex-specific manner: an example in a widespread Australian songbird. *Heredity* **123**: 608–621.

Larsson A. 2014. AliView: a fast and lightweight alignment viewer and editor for large datasets. *Bioinformatics* **30**: 3276–3278.

Lee JY, Edwards SV. 2008. Divergence across Australia's Carpentarian barrier: statistical phylogeography of the red-backed fairy wren (*Malurus melanocephalus*). *Evolution* **62**: 3117–3134.

Lee JY, Joseph L, Edwards SV. 2012. A species tree for the Australo-Papuan fairy-wrens and allies (Aves: Maluridae). *Systematic Biology* **61**: 253–271.

Lischer HEL, Excoffier L. 2011. PGDSpider: an automated data conversion tool for connecting population genetics and genomics programs. *Bioinformatics* **28**: 298–299.

Liu X, Fu Y-X. 2015. Exploring population size changes using SNP frequency spectra. *Nature Genetics* **47**: 555–559.

Liu X, Fu Y-X. 2020. Stairway Plot 2: demographic history inference with folded SNP frequency spectra. *Genome Biology* **21**: 1–9.

Maddison DR, Swofford DL, Maddison WP. 1997. NEXUS: an extensible file format for systematic information. *Systematic Biology* **46**: 590–621.

Maddison WP, Maddison DR. 2019. Mesquite: a modular system for evolutionary analysis, version 3.61.

McCormack JE, Hird SM, Zellmer AJ, Carstens BC, Brumfield RT. 2013. Applications of next-generation sequencing to phylogeography and phylogenetics. *Molecular Phylogenetics and Evolution* **66**: 526–538.

McCormack JE, Tsai WL, Faircloth BC. 2016. Sequence capture of ultraconserved elements from bird museum specimens. *Molecular Ecology Resources* **16**: 1189–1203.

Melville J, Haines ML, Hale J, Chapple S, Ritchie EG. 2016. Concordance in phylogeography and ecological niche modelling identify dispersal corridors for reptiles in arid Australia. *Journal of Biogeography* **43**: 1844–1855.

Miller EF, Green RE, Balmford A, Maisano Delser P, Beyer R, Somveille M, Leonardi M, Amos W, Manica A. 2021. Bayesian skyline plots disagree with range size changes based on species distribution models for Holarctic birds. *Molecular Ecology* **30**: 3993–4004.

Mitchell KJ, Hugall AF, Heiniger H, Joseph L, Oliver PM. 2021. Disparate origins for endemic bird taxa from the 'Gondwana Rainforests' of Central Eastern Australia. *Biological Journal of the Linnean Society* **134**: 40–56.

Muscarella R, Galante PJ, Soley-Guardia M, Boria RA, Kass JM, Uriarte M, Anderson RP. 2014. ENMeval: an R package for conducting spatially independent evaluations and estimating optimal model complexity for Maxent ecological niche models. *Methods in Ecology and Evolution* **5**: 1198–1205.

Nam K, Mugal C, Nabholz B, Schielzeth H, Wolf JBW, Backström N, Künstner A, Balakrishnan CN, Heger A, Ponting CP, Clayton DF, Ellegren H. 2010. Molecular evolution of genes in avian genomes. *Genome Biology* **11**: R68.

Nei M, Li WH. 1979. Mathematical model for studying genetic variation in terms of restriction endonucleases. *Proceedings of the National Academy of Sciences* **76**: 5269–5273.

Nei M, Takahata M. 1993. Effective population size, genetic diversity and coalescence time in subdivided populations. *Journal of Molecular Evolution* **37**: 240–244.

Nguyen LT, Schmidt HA, von Haeseler A, Minh BQ. 2015. IQ-TREE: a fast and effective stochastic algorithm for estimating maximum-likelihood phylogenies. *Molecular Biology and Evolution* **32**: 268–274.

Nickerson DA, Tobe VO, Taylor SL. 1997. PolyPhred: automating the detection and genotyping of single nucleotide substitutions using fluorescence-based resequencing. *Nucleic Acids Research* **25**: 2745–2751.

Novembre J, Johnson T, Bryc K, Kutalik Z, Boyko AR, Auton A, Indap A, King KS, Bergmann S, Nelson MR, Stephens M, Bustamante CD. 2008. Genes mirror geography within Europe. *Nature* **456**: 98–101.

Oliver PM, Laver RJ, Martins FD, Pratt RC, Hunjan S, Moritz CC. 2017. A novel hotspot of vertebrate endemism and an evolutionary refugium in tropical Australia. *Diversity and Distributions* **23**: 53–66.

Oliveros CH, Field DJ, Ksepka DT, Barker FK, Aleixo A, Andersen MJ, Alstrom P, Benz BW, Braun EL, Braun MJ, Bravo GA, Brumfield RT, Chesser RT, Claramunt S, Cracraft J, Cuervo AM, Derryberry EP, Glenn TC, Harvey MG, Hosner PA, Joseph L, Kimball RT, Mack AL, Miskelly CM, Peterson AT, Robbins MB, Sheldon FH, Silveira LF, Smith BT, White ND, Moyle RG, Faircloth BC. 2019. Earth history and the passerine superradiation. *Proceedings of the National Academy of Sciences* **116**: 7916–7925.

Painter JN, Crozier RH, Poiani A, Robertson RJ, Clarke MF. 2000. Complex social organization reflects genetic structure and relatedness in the cooperatively breeding bell miner, *Manorina melanophrys*. *Molecular Ecology* **9**: 1339–1347.

Patterson N, Price AL, Reich D. 2006. Population structure and eigenanalysis. *PLoS Genetics* **2**: e190.

Peñalba JV, Joseph L, Moritz C. 2019. Current geography masks dynamic history of gene flow during speciation in northern Australian birds. *Molecular Ecology* **28**: 630–643.

Peñalba JV, Mason IJ, Schodde R, Moritz C, Joseph L. 2017. Characterizing divergence through three adjacent Australian avian transition zones. *Journal of Biogeography* **44**: 2247–2258.

Pepper M, Doughty P, Fujita MK, Moritz C, Keogh JS. 2013a. Speciation on the rocks: integrated systematics of the *Heteronotia spelea* species complex (Gekkota; Reptilia) from Western and Central Australia. *PLoS One* **8**: e78110.

Pepper M, Doughty P, Keogh JS. 2006. Molecular phylogeny and phylogeography of the Australian *Diplodactylus stenodactylus* (Gekkota; Reptilia) species-group based on mitochondrial and nuclear genes reveals an ancient split between Pilbara and non-Pilbara *D. stenodactylus*. *Molecular Phylogenetics and Evolution* **41**: 539–555.

Pepper M, Doughty P, Keogh JS. 2013b. Geodiversity and endemism in the iconic Australian Pilbara region: a review of landscape evolution and biotic response in an ancient refugium. *Journal of Biogeography* **40**: 1225–1239.

Pepper M, Fujita MK, Moritz C, Keogh JS. 2011. Palaeoclimate change drove diversification among isolated mountain refugia in the Australian arid zone. *Molecular Ecology* **20**: 1529–1545.

Pfeifer B, Wittelsburger U, Ramos-Onsins SE, Lercher MJ. 2014. PopGenome: an efficient Swiss army knife for population genomic analyses in R. *Molecular Biology and Evolution* **31**: 1929–1936.

Phillips SJ, Anderson RP, Dudík M, Schapire RE, Blair ME. 2017. Opening the black box: an open-source release of Maxent. *Ecography* **40**: 887–893.

Plummer M, Best N, Cowles K, Vines K. 2006. CODA: Convergence Diagnosis and Output Analysis for MCMC. *R News* **6**: 7–11.

Potter S, Bragg J, Peter BM, Bi K, Moritz C. 2016. Phylogenomics at the tips: inferring lineages and their demographic history in a tropical lizard, *Carlia amax*. *Molecular Ecology* **25**: 1367–1380.

Potter S, Eldridge MD, Taggart DA, Cooper SJ. 2012. Multiple biogeographical barriers identified across the Monsoon Tropics of northern Australia: phylogeographic analysis of the *brachyotis* group of rock-wallabies. *Molecular Ecology* **21**: 2254–2269.

Potter S, Silva ACA, Bragg JG, Catalano SR, Donnellan S, Doughty P, Scott ML, Moritz C. 2019. Contrasting scales of local persistence between monsoonal and arid biomes in closely related, low-dispersal vertebrates. *Journal of Biogeography* **46**: 2506–2519.

Potter S, Xue AT, Bragg JG, Rosauer DF, Roycroft EJ, Moritz C. 2018. Pleistocene climatic changes drive diversification across a tropical savanna. *Molecular Ecology* **27**: 520–532.

Pritchard JK, Stephens M, Donnelly P. 2000. Inference of population structure using multilocus genotype data. *Genetics* **155**: 945–959.

R Core Team. 2019. R: A Language and Environment for Statistical Computing. R Foundation for Statistical Computing, Vienna, Austria. https://www.R-project.org/

Rambaut A, Drummond AJ, Xie D, Baele G, Suchard MA. 2018. Posterior summarization in Bayesian phylogenetics using Tracer 1.7. *Systematic Biology* **67**: 901–904.

Rannala B, Yang Z. 2017. Efficient Bayesian species tree inference under the multispecies coalescent. *Systematic Biology* **66**: 823–842.

Reeves JM, Bostock HC, Ayliffe LK, Barrows TT, De Deckker P, Devriendt LS, Dunbar GB, Drysdale RN, Fitzsimmons KE, Gagan MK, Griffiths ML, Haberle SG, Jansen JD, Krause C, Lewis S, McGregor HV, Mooney SD, Moss P, Nanson GC, Purcell A, van der Kaars S. 2013. Palaeoenvironmental change in tropical Australasia over the last 30,000 years - a synthesis by the OZ-INTIMATE group. *Quaternary Science Reviews* **74**: 97–114.

Rockman MV, Wray GA. 2002. Abundant raw material for cis-regulatory evolution in humans. *Molecular Biology and Evolution* **19**: 1991–2004.

Rosauer DF, Byrne M, Blom MPK, Coates DJ, Donnellan S, Doughty P, Keogh JS, Kinloch J, Laver RJ, Myers C, Oliver PM, Potter S, Rabosky DL, Silva ACA, Smith J, Moritz C. 2018. Real-world conservation planning for evolutionary diversity in the Kimberley, Australia, sidesteps uncertain taxonomy. *Conservation Letters* **11**:e12438.

Rusk CL, Walters EL, Koenig WD. 2013. Cooperative breeding and long-distance dispersal: a test using vagrant records. *PLoS One* **8**: e58624.

Schaeffer SW. 2002. Molecular population genetics of sequence length diversity in the *Adh* region of *Drosophila pseudoobscura*. *Genetical Research* **80**: 163–175.

Shimodaira H. 2002. An approximately unbiased test of phylogenetic tree selection. *Systematic Biology* **51**: 492–508.

Silva ACA, Santos N, Ogilvie HA, Moritz C. 2017. Validation and description of two new north-western Australian rainbow skinks with multispecies coalescent methods and morphology. *PeerJ* **5**:e3724. https://doi.org/10.7717/peerj.3724

Slatkin M, Maddison WP. 1989. A cladistic measure of gene flow inferred from the phylogenies of alleles. *Genetics* **123**: 603–613.

Stephens M, Smith NJ, Donnelly P. 2001. A new statistical method for haplotype reconstruction from population data. *American Journal of Human Genetics* **68**: 978–989.

Stiels D, Schidelko K. 2018. Modeling avian distributions and niches: insights into invasions and speciation in birds. In: Tietze DT, ed. *Bird species: how they arise, modify and vanish*. Cham: Springer International Publishing, 147–164.

Swofford DL. 2002. *Phylogenetic analysis using parsimony (* and other methods). Version 4*. Sunderland: Sinauer Associates.

Tajima F. 1989. Statistical method for testing the neutral mutation hypothesis by DNA polymorphism. *Genetics* **123**: 585–595.

Takahata N. 1989. Gene genealogy in three related populations: consistency probability between gene and population trees. *Genetics* **122**: 957–966.

Termignoni-García F, Kirchman JJ, Clark J, Edwards Scott V. 2022. Comparative population genomics of cryptic speciation and adaptive divergence in Bicknell's and gray-cheeked thrushes (Aves: *Catharus bicknelli* and *Catharus minimus*). *Genome Biology and Evolution* **14**: evab255, https://doi.org/10.1093/gbe/evab255

Turner TL, Hahn MW. 2010. Genomic islands of speciation or genomic islands and speciation? *Molecular Ecology* **19**: 848–850.

Umbrello LS, Didham RK, How RA, Huey JA. 2020. Multi-species phylogeography of arid-zone Sminthopsinae (Marsupialia: Dasyuridae) reveals evidence of refugia and population expansion in response to quaternary change. *Genes* **11**: 963.

Unmack PJ, Adams M, Hammer MP, Johnson JB, Gruber B, Gilles A, Young M, Georges A. 2021. Plotting for change: an analytical framework to aid decisions on which lineages are candidate species in phylogenomic species discovery. *Biological Journal of the Linnean Society* **135**: 117–137.

Warren DL, Dornburg A, Zapfe K, Iglesias TL. 2021. The effects of climate change on Australia's only endemic Pokémon: measuring bias in species distribution models. *Methods in Ecology and Evolution* **12**: 985–995.

Wilson AC, Cann RL, Carr SM, George M, Gyllensten UB, Helm-Bychowski KM, Higuchi RG, Palumbi SR, Prager EM, Sage RD, Stoneking M. 1985. Mitochondrial DNA and two perspectives on evolutionary genetics. *Biological Journal of the Linnaean Society* **26**: 375–400.

Yang R-C. 1998. Estimating hierarchical F-statistics. *Evolution* **52**: 950–956.

Yang Z, Rannala B. 2010. Bayesian species delimitation using multilocus sequence data. *Proceedings of the National Academy of Sciences* **107**: 9264–9269.

Zizka A, Silvestro D, Andermann T, Azevedo J, Duarte Ritter C, Edler D, Farooq H, Herdean A, Ariza M, Scharn R, Svantesson S, Wengström N, Zizka V, Antonelli A. 2019. CoordinateCleaner: standardized cleaning of occurrence records from biological collection databases. *Methods in Ecology and Evolution* **10**: 744–751.

SUPPORTING INFORMATION

Additional supporting information may be found in the online version of this article on the publisher's website.

Text S1. Fieldwork, sampling and taxa studied; DNA isolation, primer development and resequencing; Phrapl analysis; approximately unbiased test; simulations using ms; results of coalescent simulations using ms; analyses using the site frequency spectrum.

Fig. S1. Maximum likelihood tree of control region I sequences (373 bp) of *C. picumnus* and *C. melanurus* using IQ-Tree.

Fig. S2. Maximum likelihood consensus tree of control region I sequences using IQ-Tree.

Fig. S3. Maximum likelihood gene trees, showing extent of or lack of species monophyly for each of the 14 anonymous loci (AL).
Fig. S4. Heatmap showing results of approximately unbiased tests of each of the 14 anonymous loci against the best trees of the other 13 loci.
Fig. S5. Results of simulations using ms and comparison with observed number of interspecific coalescent events (ICEs).
Fig. S6. Heatmap showing values of mtDNA F_{st} (below diagonal) or d_{xy} (above diagonal) between each pair of populations in *C. picumnus* and *C. melanurus* as calculated with PopGenome.
Fig. S7. Heatmap showing values of F_{st} (below diagonal) or d_{xy} (above diagonal) between each pair of populations in *C. picumnus* and *C. melanurus* as calculated with PopGenome.
Fig. S8. Comparison of F_{st} for indels and SNPs between populations of *C. picumnus* and *C. melanurus*.
Fig. S9. Summary of the best model estimated by bpp analyses.
Fig. S10. Correlation between nucleotide diversity (π) per locus as estimated in PopGenome.
Fig. S11. Models of within-species population structure used in migrate-n analysis.
Fig. S12. Eight two-species divergence and divergence with gene flow (1–8) models and one equilibrium migration model (9) used with migrate-n.
Fig. S13. The thinned localities from GBIF used to generate niche models, with expert range maps in the background (*C. picumnus*, $N = 499$), *C. melanurus*, $N = 243$).
Fig. S14. Estimated range areas for *C. picumnus*, *C. melanurus*, *C. rufa* and *C. affinis* for time periods from the Anthropocene (left) to the mid-Pliocene (right).
Fig. S15. Estimated proportion of range overlaps between pairs of *Climacteris* species through geological epochs.
Table S1. Tissue samples used in analysis of nuclear and mitochondrial DNA of treecreepers (all specimens genus *Climacteris*).
Table S2. List of BLAST hits for those queries of anonymous loci that returned a significant hit.
Table S3. Characteristics of anonymous loci and mtDNA control region 1 variation.
Table S4. Results of Phrapl analysis of ten models ('params.vector') with divergence ('collapse'), interspecific gene flow ('migration') and population size changes ('n0multiplier').
Table S5. Characteristics of insertion-deletion polymorphisms within and among *Climacteris* species.
Table S6. Parameter estimates of bpp analysis of *C. picumnus* and *C. melanurus*, divergence and divergence with pulse migration models.
Table S7. Bayes factor tests of models of divergence and divergence with pulse-gene flow using bpp.
Table S8. Migrate-n parameter estimates, within and between species.
Table S9. Bayes factor tests of within- and between-species phylogeographic models with migrate-n.
Table S10. Different methods of calculating the site frequency spectrum in *C. picumnus* and *C. melanurus*.
Table S11. Estimates of effective population size through time from Stairway analyses using four different methods for calculating the folded or unfolded site frequency spectrum.
Table S12. Summary of linear models linking changes in population size over time from Stairway analyses and estimated ancestral habitable area from environmental niche models.